JOC The Journal of Organic Chemistry

ARTICLE

pubs.acs.org/joc

Synthesis and Properties of Conjugated Oligoyne-Centered π-Extended Tetrathiafulvalene Analogues and Related Macromolecular Systems

Guang Chen,[†] Ilias Mahmud,[†] Louise N. Dawe,[†] Lee M. Daniels,[‡] and Yuming Zhao*[,†]

[†]Department of Chemistry, Memorial University of Newfoundland, St. John's, Newfoundland A1B 3X7, Canada

[‡]Rigaku Americas Corporation, 9009 New Trails Drive, The Woodlands, Texas 77381, United States

Supporting Information

ABSTRACT: Alkynyl-substituted phenyldithiafulvenes have been found to act as versatile building blocks for the construction of π-conjugated molecular rods, shape-persistent macrocycles (SPMs), and conducting polymers. Through Cu(I)-catalyzed alkynyl homocoupling, a series of linear-shaped π-extended tetrathiafulvalene analogues (exTTFs) carrying conjugated oligoynes (ranging from diyne to hexayne) as the central π-bridge were readily prepared. The solid-state properties and reactivities of diyne- and tetrayne-centered exTTFs were characterized by X-ray crystallography and differential scanning calorimetry (DSC), while the electronic properties of the oligoyne-exTTFs were elucidated by UV−vis absorption spectroscopy and density functional theory (DFT) calculations. Cyclic voltammetric analysis showed that the terminal phenyldithiafulvene groups of the oligyne-exTTFs could undergo oxidative coupling to form tetrathiafulvalene vinylogue (TTFV)-linked polymer wires. Through a different synthetic route involving oxidative dimerization and Pd/Cu-catalyzed alkynyl homocoupling, the acetylenic phenyldithiafulvene precursors led to shape-persistent macrocycles where the formation of trimeric macrocycles was particularly favored due to the small ring strain incurred. Finally, spectroelectrochemical studies on these oligoyne and TTF hybrid materials disclosed electrochromic and molecular redox-controlled switching properties applicable to molecular electronic and optoelectronic devices.

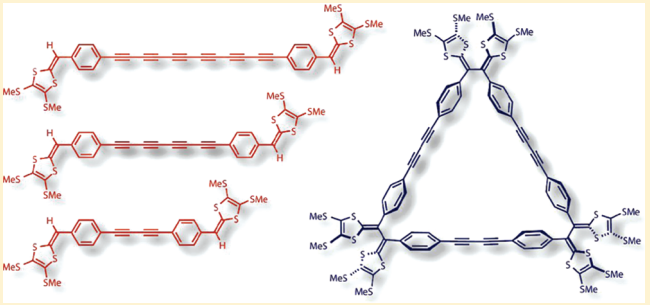

INTRODUCTION

Tetrathiafulvalene (TTF) as an important organic electron donor has found extensive uses in modern materials science.[1,2] Ever since the seminal work by Wudl and co-workers on the electrical conductivity of $[TTF]^{\bullet+}Cl^{-}$ in the early 1970s,[3,4] an enormous array of TTF variants has been synthesized and applied as useful building blocks in the construction of advanced molecular/supramolecular materials and devices, ranging from organic conductors and superconductors,[5−8] magnets,[7−9] molecular switches and sensors,[10−12] molecular machines,[13,14] organic optoelectronics,[15,16] and plastic solar cells,[15,17,18] just to name a few. In the development of functional TTF derivatives, the strategy of increasing the π-conjugation of the TTF backbone has been widely employed to generate the so-called π-extended tetrathiafulvalene analogues (exTTFs),[11,15,19,20] In current TTF chemistry, insertion of various π-conjugated spacers such as quinoid,[21−24] vinylogous,[25−27] arylene,[28] and acetylene bridges[29,30] between the two dithiole rings of TTF has been proven effective at tuning the properties and functions of exTTF derivatives to be applicable for device applications, such as enhanced electron-donating ability, increased solid-state ordering and dimensionality, as well as controlled multistage redox activities.

Conjugated oligoynes or polyynes constitute a class of quasi-one-dimensional conjugated carbon chains and have been extensively investigated as versatile scaffoldings for functional carbon-rich materials, owing to their rich optoelectronic and electromagnetic properties and unique solid-state reactivities.[31−39] For instance, the nonlinear optical susceptibilities of oligoynes were found to increase exponentially with increasing number of acetylenic repeat units,[40,41] while topochemical polymerization of oligoynes tended to result in highly conjugated polymer networks[37,42−50] and ordered carbon-based nanomaterials.[51−54] Moreover, the "wire-like" sp carbon chains (spCCs) of conjugated oligoynes or polyynes are the substructures of an intriguing carbon allotrope−carbyne,[55,56] while debates over the nature of electronic delocalization in spCCs have galvanized both experimental and theoretical investigations.[57−63] In particular, synthetic endeavors aiming at extension and functionalization of conjugated oligoynes have been actively undertaken in recent years in order to realize suitable models for unraveling the mystical characteristics of carbyne and related polyyne materials.[63−70]

Received: January 12, 2011
Published: March 08, 2011

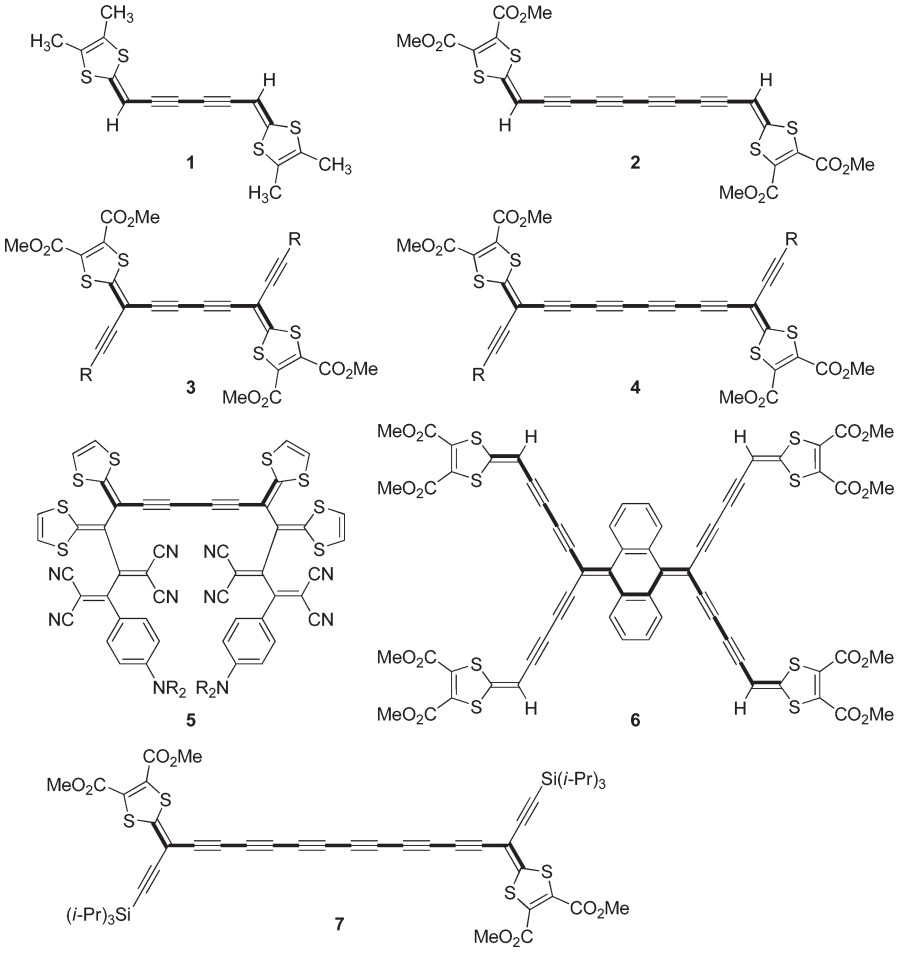

Figure 1. Examples of conjugated oligoyne-centered exTTFs reported in the literature.

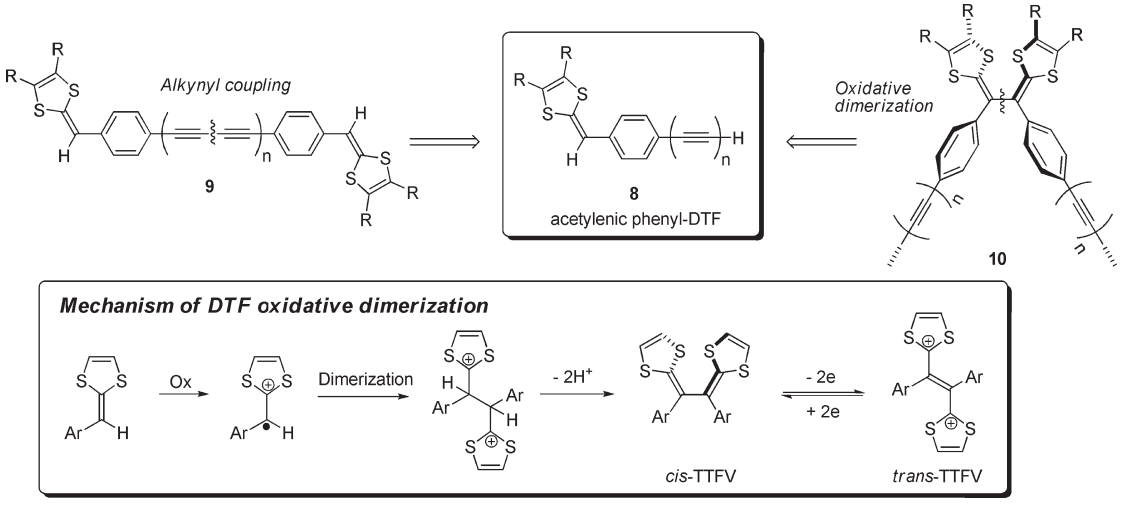

Figure 2. Versatile reactivities of acetylenic phenyl-DTF.

Oligoyne-extended TTF analogues have been synthesized and studied for more than two decades; however, they still remain a rather small branch in the vast family of exTTF derivatives.[71−74] In 1990, Gorgues and co-workers reported the synthesis of a bis(dithiafulvenyl)-end-capped conjugated 1,3-butadiyne **1** (Figure 1) by a Wittig−Horner reaction.[75,76] The dithiafulvenyl (DTF) moieties of **1** are in direct conjugation via a diyne π-spacer (highlighted bold in Figure 1), presenting the first example of a diyne-centered exTTF. The synthesis of 1,3,5,7-octatetrayne-centered exTTF **2**, which is a longer homologue of exTTF **1**, was, however, accomplished at a much later time. In 2004, Nielsen and co-workers used a Cu-catalyzed homocoupling

dx.doi.org/10.1021/jo2000447 |J. Org. Chem. 2011, 76, 2701–2715

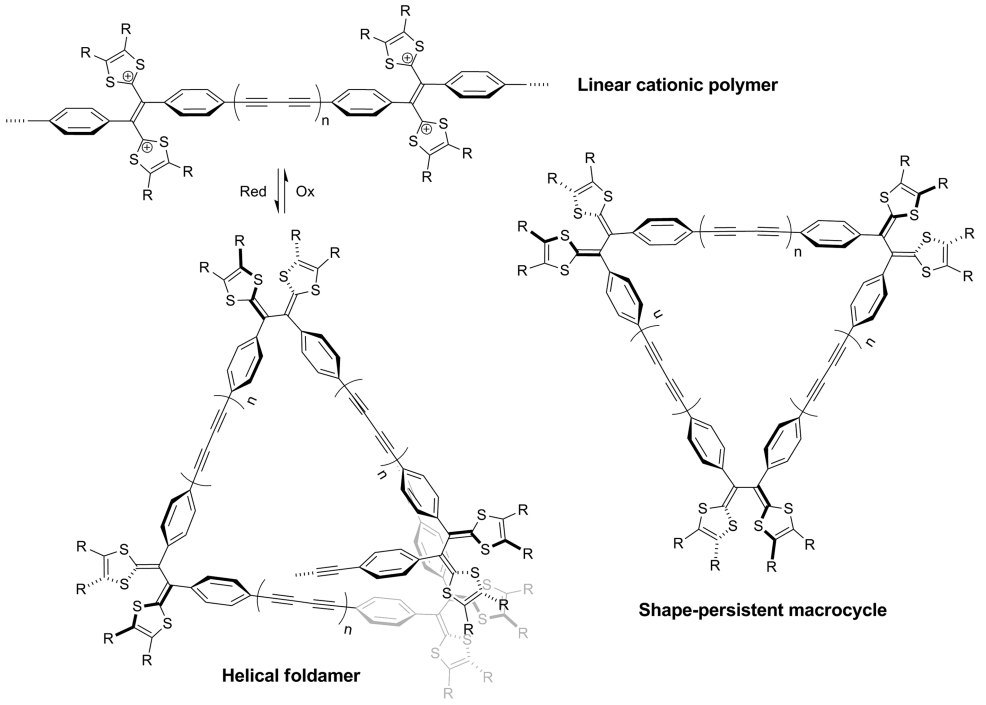

Figure 3. Different macromolecular systems possibly derived from acetylenic phenyl-DTF **8**.

reaction to construct tetrayne-exTTF **2** and investigated its redox properties by electrochemical analysis.[77] A similar series of diyne- and tetrayne-centered exTTFs **3** and **4** have been prepared and investigated by Diederich and Nielsen.[78,79] In these compounds, extended acetylenic units were appended to the exTTF backbones in a cross-conjugated manner. Very recently, Diederich and co-workers reported the synthesis of a diyne-centered exTTF **5** via successive TTF/TCNE cycloadditions on a conjugated hexayne precursor.[80] In 2007, Nielsen and co-workers reported an exTTF derivative **6** by oxidative alkynyl coupling reactions.[81] The highlighted conjugation path of **6** shown in Figure 1 clearly reveals an exTTF segment, in which two DTF groups are connected through a linearly conjugated diyne-quinoid-diyne π-bridge. In addition to diyne and tetrayne units, Nielsen and co-workers also successfully prepared a hexayne-centered exTTF **7** in good yield via Hay coupling.[77] Although the chemical stability of hexayne **7** was not mentioned in detail, the successful separation and spectroscopic characterization of hexayne **7** were remarkable, given the relatively poor stability of many hexayne species.[82] The sufficient stability can be attributed to the presence of bulky triisopropylsilyl (TIPS) end-capping groups that prevent decomposition of the central hexayne unit.[63]

Given the limited number of oligoyne-centered exTTFs in the current literature, continued synthesis and characterization of new oligoyne-exTTFs are indispensable and beneficial to better understanding of the fundamental structure−property relationships and potential applications of electroactive oligoynes in synthetic and materials chemistry. Upon this consideration, we set out to investigate a series of oligoyne-centered exTTFs **9** (Figure 2). The basic structure of **9** is akin to those of exTTFs **1** and **2**; however, the incorporation of a phenyl ring between the DTF and alkynyl groups in our designed structure not only elongates π-conjugation but also adds versatile reactivity allowing for the construction of highly conjugated macromolecular systems. The DTF molecules have been known to undergo an oxidative dimerization reaction to form tetrathiafulvalene vinylogues (TTFVs).[6,83−91] As illustrated in the mechanism in Figure 2, the key step of this reaction involves the formation of the DTF radical cation, which requires the assistance of a neighboring group to gain sufficient stability for subsequent dimerization.[87,92] In general, DTF compounds that are monosubstituted with aryl or electron-withdrawing groups are readily subjected to oxidative dimerization reactions, whereas the alkynyl-substituted DTF species has not been known to undergo this type of reaction. In studying the electrochemistry of an acceptor-substituted acetylenic DTF, Nielsen and co-workers observed the formation of a blue-colored thin film on the surface of the working electrode.[93] The authors suggested the thin film be an insoluble cationic species; however, the possibility of electropolymerization cannot be simply ruled out and its occurrence still remains unclear. In our design, the two phenyl-DTF units in oligoyne-exTTF **9** serve as a pair of facile synthetic handles for cross-linking through the oxidative coupling reaction to generate some intriguing conjugated polymer materials.

A straightforward retro-synthetic analysis of oligoyne-exTTF **9** leads to a handy synthon, acetylenic phenyl-DTF **8**, which in turn can be used to make other varieties of TTFV-based macromolecular structures through sequential DTF dimerization and alkynyl coupling reactions. Of particular note is that the diphenyl-substituted TTFV unit shows redox-controlled conformational switching properties.[86,87] In the neutral state, the two phenyl groups are oriented in a *cis*, V-shaped conformation governed by steric crowding, whereas upon oxidation the dication of phenyl-TTF assumes a *trans* conformation where the two phenyl groups point outwardly in a linear fashion as a result of the on-site Coulombic repulsion between the two cationic dithiolium rings.[94−97] In this vein, it is conceivable that structural extension based on synthon **8** would result in macromolecules of very different conformations, depending on the synthetic sequences and conditions. Taking the V-shape of neutral diphenyl-TTFV and

dx.doi.org/10.1021/jo2000447 |*J. Org. Chem.* 2011, 76, 2701–2715

Scheme 1. Synthesis Oligoyne-Centered exTTFs 16−18

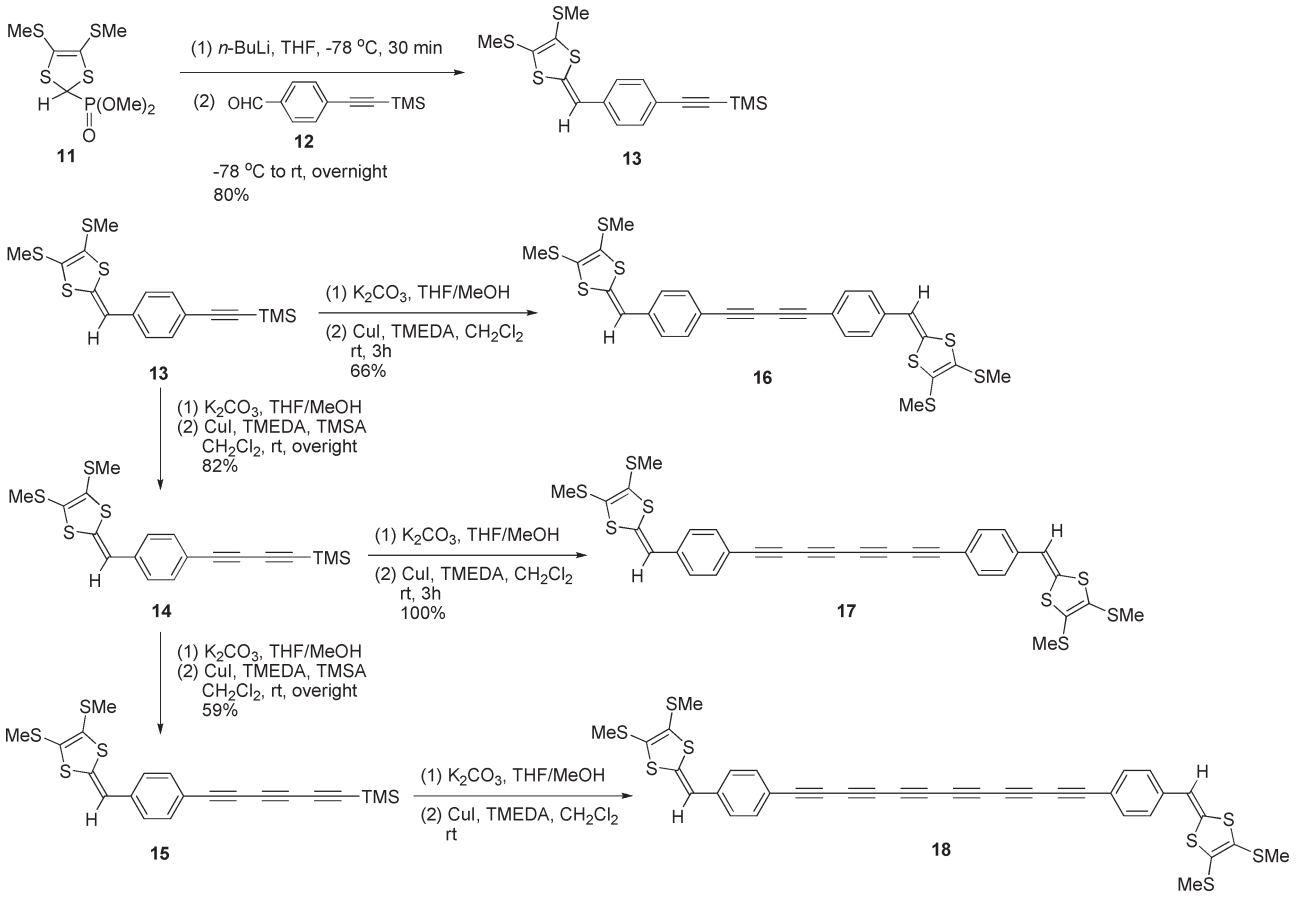

the linear shape of oligoyne and dicationic [phenyl-TTFV]$^{2+}$ units into account, three major synthetic consequences are readily perceived as illustrated in Figure 3, namely linear cationic polymer chains, helical foldamers,[98] and shape-persistent macrocycles (SPMs).[99−102] These oligoyne-TTFV-related macromolecules have not been known in the literature prior to our work. In a recent paper, we reported the synthesis and properties of a diyne-based exTTF and related polymers and macrocycles.[103] This paper describes our further investigations of oligoyne-centered exTTFs, ranging from diyne to hexayne analogues. In addition, related oligoyne-TTFV polymers and SPMs were prepared and their properties were characterized by spectroscopic and voltammetric techniques.

RESULTS AND DISCUSSION

Synthesis. The synthesis of oligoyne-centered exTTFs is outlined in Scheme 1. Phosphonate **11**[30,103−106] was first treated with *n*-BuLi in THF at low temperature to form the corresponding ylide, which was immediately reacted with benzaldehyde **12** through a Horner−Wadsworth−Emmons (HWE) reaction to give acetylenic phenyl-DTF **13** in 80% yield. DTF **13** was desilylated with K_2CO_3 affording a free alkyne intermediate, which was subjected to Hay coupling[107] with excess TMSA (ca. 14 mol equiv) to form diyne-attached phenyl-DTF **14** in 82% yield. Repetition of the same desilylation/Hay coupling sequence on **14** led to the formation of triyne-substituted phenyl-DTF **15**. In the Hay coupling reaction, a considerably large excess of TMSA (ca. 38 mol equiv) was added to ensure a satisfactory yield of 59%. With the acetylenic DTF precursors **13**−**15** in hand, a straightforward oxidative homocoupling strategy was then implemented to produce the desired oligoyne-centered exTTFs. As shown in Scheme 1, desilylation of DTF **13** with K_2CO_3 followed by oxidative homocoupling in the presence of the Hay catalyst (CuI/TMEDA) afforded diyne-centered exTTF **16** in 66% yield. Under the same conditions, the homocoupling of desilylated diyne-DTF **14** proceeded more rapidly and efficiently, resulting in tetrayne-centered exTTF **17** in a quantitative yield. Similarly, the homocoupling of desilylated triyne-DTF **15** also resulted in a high yield of hexayne-exTTF **18** in dilute solution as evidenced by thin-layer chromatography (TLC). MALDI-TOF MS analysis clearly showed the molecular ion at m/z = 709.9461 corresponding to [**18**]$^+$ (709.9487 calcd for $C_{36}H_{22}S_8$), substantiating the formation of hexayne-exTTF **18** during the homocoupling reaction (see the Supporting Information). The isolation of hexayne-exTTF **18** was, however, unsuccessful due to its extremely poor chemical stability in the solid state. Actually, upon evaporation of the solvent under vacuum, the orange-colored solution of **18** was instantaneously changed into a purplish substance which was insoluble in any organic solvents. The insolubility of the solid products hampered meaningful structural elucidation. Previously, Tykwinski and co-workers synthesized a diphenyl-end-capped hexayne which was isolated as a relatively stable orange solid.[40] In our case, the dramatically reduced stability

dx.doi.org/10.1021/jo2000447 |J. Org. Chem. 2011, 76, 2701–2715

Scheme 2. Synthesis of Shape-Persistent Macrocycles 21 and 22

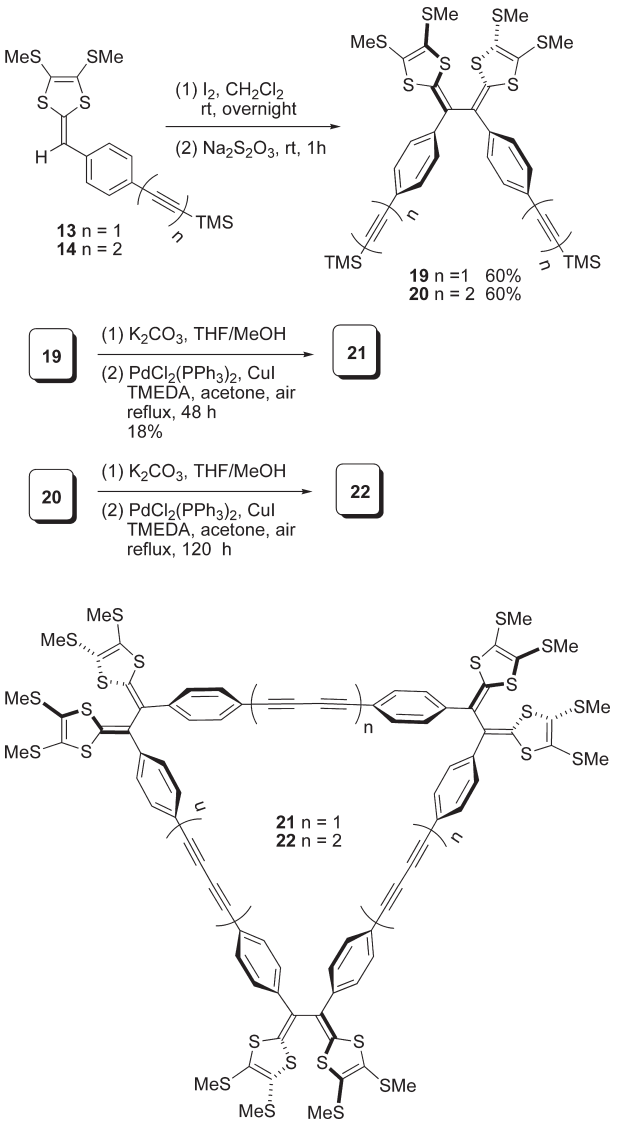

of hexayne **18** can be tentatively attributed to the end-capping DTF groups that may induce optimal solid-state packing geometry via strong S−S contacts to facilitate topochemical polymerization. On the other hand, nucleophilic attack of the SMe substituents to the hexayne moiety may also take place to a certain extent to destabilize hexayne **18**. The exact reason for the instability of **18** in the solid state is unclear at this juncture and awaits further investigation.

Apart from the "rod-like" oligoyne-exTTF motifs, the construction of shape-persistent macrocycles was also explored in our synthetic work using the acetylenic phenyl-DTFs as precursors. As shown in Scheme 2, phenyl-DTFs **13** and **14** were respectively subjected to an iodine-promoted oxidative dimerization reaction,[90,108] yielding cationic dimerized products which were subsequently treated with $Na_2S_2O_3$ to afford neutral acetylenic phenyl-TTFVs **19** and **20** in the same yield of 60%. At this juncture, a straightforward desilylation/homocoupling route should furnish macrocyclic products. The use of Cu(I) species, such as CuCl or CuI, as the metal-based catalyst for homocoupling was first attempted; however, these conditions resulted in very poor yields for the macrocyclization reaction. After a number of trials, a Cu(I)/Pd(II) cocatalyst system similar to the one employed in the synthesis of TTF-based [18]annulenes reported by Iyoda et al.[109] was found to give the best outcomes. In our work, desilylation of TTFV **19** with K_2CO_3 followed by a Pd/Cu-catalyzed homocoupling reaction under dilute conditions (ca. 2.8 mM) in acetone under reflux for 2 days afforded a series of macrocyclic products ranging from trimer to pentamer, as evidenced by MALDI-TOF MS analysis (Figure 4A). Flash column chromatography successfully isolated trimeric macrocycle **21** as the major product in 18% yield, while other byproducts were not separable due to their trace amounts.

In a similar manner, TTFV **20** was desilylated and then subjected to macrocyclization reactions under the catalysis of Pd/Cu in refluxing acetone for 5 days (see Scheme 2). MALDI-TOF MS analysis clearly showed the formation of macrocycle **22** as the major product of the macrocyclization (see Figure 4B). However, efforts to isolate pure **22** by flash column chromatography failed because of the very similar R_f value of **22** to those of some inextricable byproducts.

The two phenyl-DTF units in oligoyne-exTTFs **16** and **17** were expected to cross-link into "chain-like" oligomer and polymer wires upon oxidative dimerization. The oxidative coupling of DTF groups could be conducted by either chemical or electrochemical means. Chemical polymerization was performed by treating the solution of **16** or **17** with molecular iodine in CH_2Cl_2 at ambient temperature for ca. 12 h (see Scheme 3).[90,108] Afterward, the resulting polymers were reduced by $Na_2S_2O_3$ to afford neutral polymer products **P1** and **P2**, respectively. Both **P1** and **P2** are orange solids and readily soluble in nonpolar organic solvents such as CH_2Cl_2 and chloroform. MALDI-TOF MS analysis on the samples of **P1** and **P2** revealed the presence of oligomers of short chain lengths (m = 2−8 for **P1** and m = 2−4 for **P2**, see the Supporting Information). The relatively low degrees of polymerization observed are not surprising given the moderate yields of the iodine-induced DTF coupling in the solution phase. In addition, electrochemical polymerization of oligoyne-exTTFs **16** and **17** could be readily achieved via electrodeposition on conductive substrates under standard voltammetric or electrolysis conditions.[84,85] The electrochemically polymerized products formed high-quality thin films on the surface of the working electrode, which were not soluble in common organic solvents. These results indicated that electropolymerization tended to induce much higher degrees of polymerization than did the chemical method. The detailed results of the electrochemically induced polymerization of oligoyne-exTTFs **16** and **17** will be elaborated in the latter section.

Structural and Solid-State Properties. Single crystals of diyne-exTTF **16** and tetrayne-exTTF **17** were grown by slow solvent evaporation methods at low temperature (−4 °C), and their detailed molecular and solid-state structures were characterized by single-crystal X-ray crystallography. Both diyne-exTTF **16** and tetrayne-exTTF **17** show a nearly planar π-conjugated backbone in the molecular structure (Figure 5A, B), with the DTF rings slightly deviated from the plane of the phenyl rings by ca. 15−20°. The X-ray structure of diyne **16** is in good agreement with the optimized molecular geometries obtained from density functional theory (DFT) calculations at the B3LYP/6-31G* level of theory. For tetrayne **17**, however, the theoretically predicted triple bond distances appear to be slightly longer than the crystallographic values by ca. 0.02 Å (see the

dx.doi.org/10.1021/jo2000447 |J. Org. Chem. 2011, 76, 2701–2715

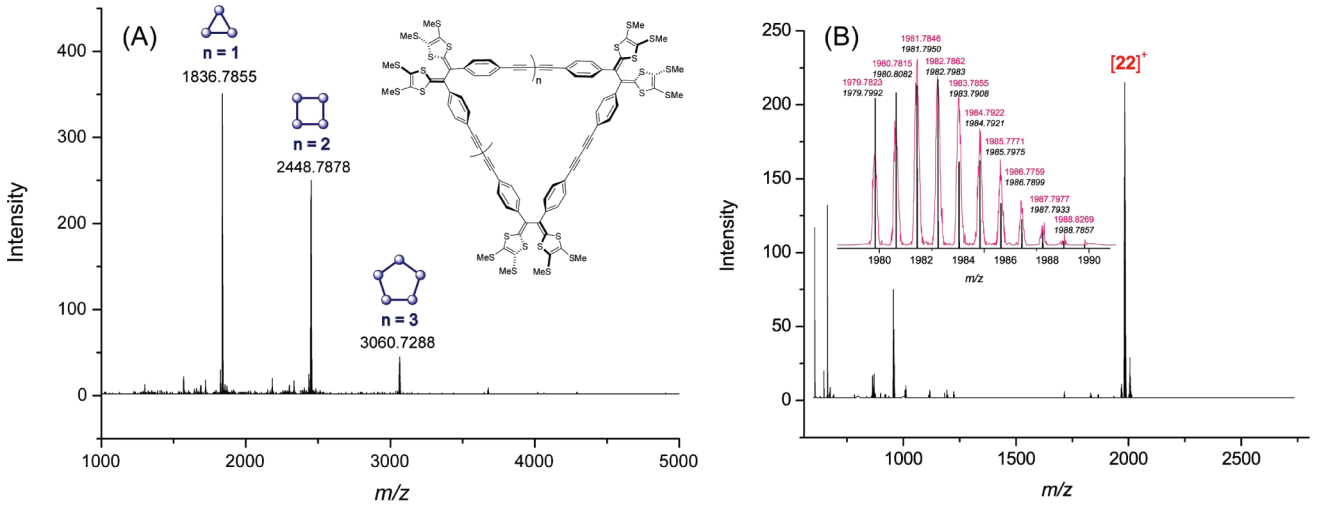

Figure 4. (A) MALDI-TOF MS analysis of the crude reaction mixture of the synthesis of macrocycle **21**. (B) MALDI-TOF mass spectrum of macrocycle **22**. The inset compares the experimentally determined isotope envelop of molecular ion $[\mathbf{22}]^+$ (pink color) against theoretically calculated pattern (black color).

Scheme 3. Synthesis of Poly(oligoyne-TTFV)s P1 and P2 via DTF Oxidative Coupling

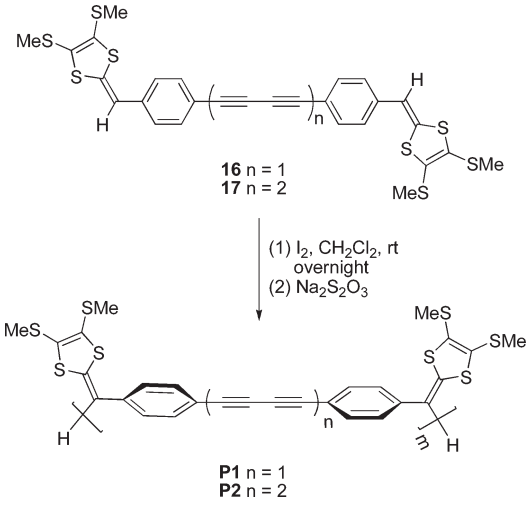

Supporting Information). The discrepancy stems from the well-known fact that the B3LYP method tends to overestimate the degree of electron delocalization for some linearly conjugated systems,[110−112] and hence, predictions on the structural properties of higher conjugated oligoynes and polyynes by this method should be treated with caution.

In the crystal lattice, molecules of diyne-exTTF **16** are closely packed at a distance of d = 5.35 Å with an inclination angle ϕ = 57.2° between the axes of molecules and the packing axis (see Figure 5C, E), while the distances between the nearest parallel diyne chains (C1′−C2 4.79 Å, C1′−C4 4.59 Å) are beyond the range of van der Waals contact (ca. 3.4 Å). Such packing geometries are moderately deviated from the optimal arrangements for diacetylene 1,4-addition (d = 3.5 Å, C1′−C4 = 3.5−4.0 Å, ϕ= 45°)[37,44,46] polymerization and therefore suggest a low probability for diyne **16** to react by topochemically controlled polymerization in the solid state. The single crystals of tetrayne-exTTF **17** show a packing distance d = 5.34 Å similar to that of diyne **16**, but a relatively smaller inclination angle ϕ = 48.8°. Of note is that the C1′ to C4 distance (4.30 Å) is considerably shorter than those of C1′ to C2 and C1′ to C6, which implies a higher probability for topochemical polymerization in a 1,4-addition fashion. In addition to the ordered alignment of oligoyne moieties, intimate S−S interactions stand out as another notable feature in the solid-state structure. In the crystal of diyne-exTTF **16**, the shortest S−S distances between adjacent molecules are 3.51 Å, while for tetrayne-exTTF **17** the close S−S contacts are 3.99 and 4.04 Å. Clearly, the DTF rings play an important role in dictating the solid-state packing properties of oligoyne-exTTFs, which in turn affect their solid-state reactivity. The close S−S interactions are believed to be responsible for the observed poor stability of hexayne-exTTF **18** in the solid state.

To further explore the solid-state thermal reactivities of oligoyne-exTTFs **16** and **17**, differential scanning calorimetry (DSC) and thermogravimetric analysis (TGA) were undertaken. As shown in Figure 6A, the DSC trace of diyne **16** shows a sharp endothermic peak at 206.8 °C (ΔH = −40.3 kJ/mol) which is attributed to the melting process. The melting is followed by a conspicuous exotherm at 244.5 °C (ΔH = 171.4 kJ/mol), and TGA measurement shows no significant weight loss at this temperature (see the Supporting Information). These results suggest that the exothermic process is due to the thermally induced diacetylene polymerization reaction. Given the relatively broad peak width and moderate reaction heat, the thermal polymerization very likely took place in a random and disordered manner rather than topochemical. The DSC trace of tetrayne **17** (Figure 6B) shows a noticeable endothermic transition at 137 °C, the origin of which is likely due to loss of the solvent molecules trapped in the crystal lattice rather than melting. At 226.9 °C, an intense sharp exothermic peak emerges (ΔH = 249.7 kJ/mol), while TGA data reveal a slight weight loss (ca. 10%) at this temperature. Collectively, the thermal data suggest that tetrayne **17** must have undergone an ordered polymerization pathway in the solid state. According to the crystallographic packing data (vide supra), the solid-state reaction quite possibly proceeds through the 1,4-addition of tetraynes.

The structural properties of macrocycle **21** were investigated by theoretical modeling studies. The relatively large molec ular size prevented the use of sophisticated ab initio or DFT

dx.doi.org/10.1021/jo2000447 |J. Org. Chem. 2011, 76, 2701–2715

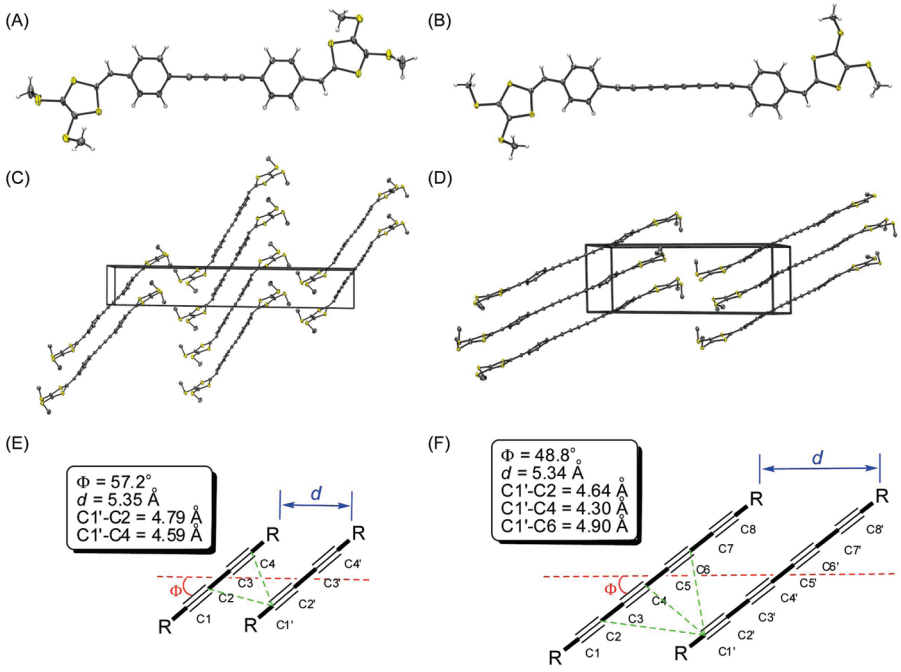

Figure 5. (A) ORTEP drawing of diyne-exTTF **16** (30% probability thermal ellipsoids). (B) ORTEP drawing of diyne-exTTF **17** (30% probability thermal ellipsoids). (C) Crystal packing of **16** viewed perpendicular to the *b*-axis. (D) Crystal packing of **17** viewed perpendicular to the *b*-axis. (E) Packing geometry of **16** in the solid state. (F) Packing geometry of **17** in the solid state.

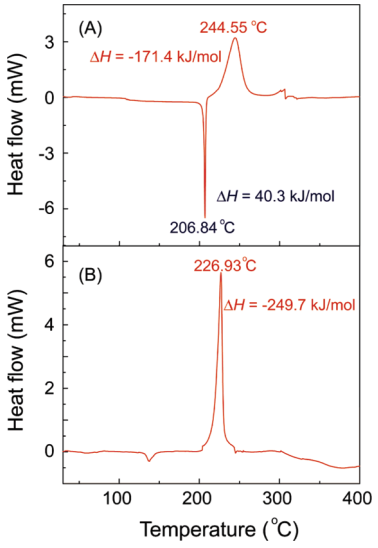

Figure 6. DSC traces of (A) diyne-exTTF **16** and (B) tetrayne exTTF **17** acquired at a scan rate of 10 °C min^{-1} in N_2 atmosphere.

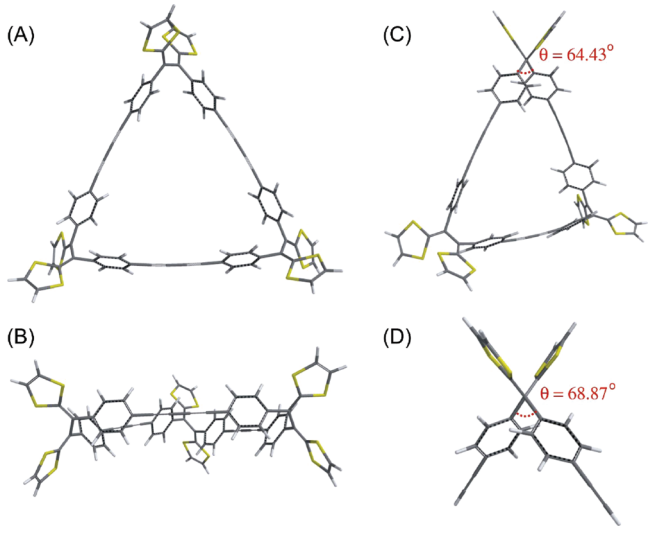

Figure 7. Molecular models of macrocycle **21**: (A) front view, (B) side view, (C) side view showing the twist angle of TTFV moiety, and (D) molecular model of phenyl-TTFV precursor. Structures are optimized at the RM1 level of theory, and the SMe groups were replaced by H atoms to reduce computational expenses.

approaches; nevertheless, semiempirical calculations based on a reparameterized AM1 method (RM1)[113] were conducted at reasonable computational expenses, and the results provided qualitative understanding on its molecular structural properties. As shown in Figure 7A, macrocycle **21** assumes a triangular-shaped ring framework. A side view of its optimized structure (Figure 7B) shows that the phenyl-oligoyne segments are in a nearly planar arrangement without significant distortion. The phenyl-TTFV units, however, adopt a nonplanar conformation with a twist angle of 64.4° (see Figure 7C). Compared with the optimized structure of its alkynyl phenyl-TTFV precursor (Figure 7D), the twist angle of macrocycle **21** appears to be only slightly reduced by about 4°. The small degree of structural reorganization suggests that the assembly of macrocycle **21** does not suffer from a substantial energetic penalty stemming from ring strain. The amount of strain energy gained is calculated to be 31.3 kJ/mol (7.48 kcal/mol) by an isodesmic reaction (see the Supporting Information). The reasonably small strain energy of **21** accounts well for its much higher yield than other larger-sized macrocyclic oligomers in the one-pot macrocyclization reaction (Scheme 2 and Figure 4). Nevertheless, TTFV-based cyclic

dx.doi.org/10.1021/jo2000447 |*J. Org. Chem.* 2011, 76, 2701–2715

oligomers larger than the trimer, although disfavored by sharply increased ring strain, are not unprecedented for TTFV-based macrocyclophanes. In a previous report, Lorcy and co-workers also observed an inseparable mixture of tetrameric and pentameric macrocycles resulting from electrolysis of a bis(dithiafulvenyl)benzene monomer.[87]

Electronic Properties. The electronic absorption properties of oligoyne-exTTFs **16**−**18** were investigated by UV−vis spectroscopy. For comparison purposes, the UV−vis spectra of acetylenic DTF precursors **13**−**15** were also acquired, and detailed spectroscopic results are given in Figure 8 and summarized in Table 1.

The UV−vis absorption spectrum of diyne-exTTF **16** (see Figure 8A) features a strong low-energy absorption band at 423 nm and a relatively weak band at 332 nm, which can be assigned to the $\pi\rightarrow\pi^*$ transitions at the phenyl-DTF moiety. In the spectrum of tetrayne-exTTF **17**, the lowest energy absorption band (λ_{max} = 467 nm) is notably red-shifted by ca. 40 nm relative to that of diyne **16**, as a result of extended π-conjugation. Additionally, a relatively strong high-energy absorption peak emerges at 307 nm in the spectrum of **17**, the origin of which is likely due to the $\pi\rightarrow\pi^*$ transitions at the phenyl-butadiyne-phenyl framework.[114] The UV−vis absorption spectrum of hexayne-exTTF **18** was measured from the solution obtained after a brief aqueous workup of the reaction solution. Since TLC analysis showed that crude product solution contained only a small amount of impurities, the spectrum was deemed trustworthy in offering a qualitative characterization of the electronic absorption properties of hexayne-exTTF **18**. In contrast to the structureless low-energy profiles observed in the spectra of diyne **16** and tetrayne **17**, the absorption of hexayne **18** gives rise to spectral patterns with more distinctive fine structures. In the low energy region, four absorption bands are discernible at 506, 467, 431, and 398 nm, and the intensities of these bands are relatively weak in comparison to the bands in the high-energy range. The spacings of the low energy peaks are determined to be 1650, 1788, and 1923 cm^{-1}, which are consistent with a vibrational progression resulting from exciton coupling to the C═C and C≡C stretching modes.[63,70,115] In the high energy region, fine structures composed of a number of sharp absorption peaks are also clearly seen at 343, 326, 303, 283, and 264 nm. The spacings of these peaks are 1520, 2328, 2332, and 2543 cm^{-1}, respectively, and such a spectral pattern can be assigned to the characteristic vibrational modes of phenyl-end-capped hexayne moiety.[63,70]

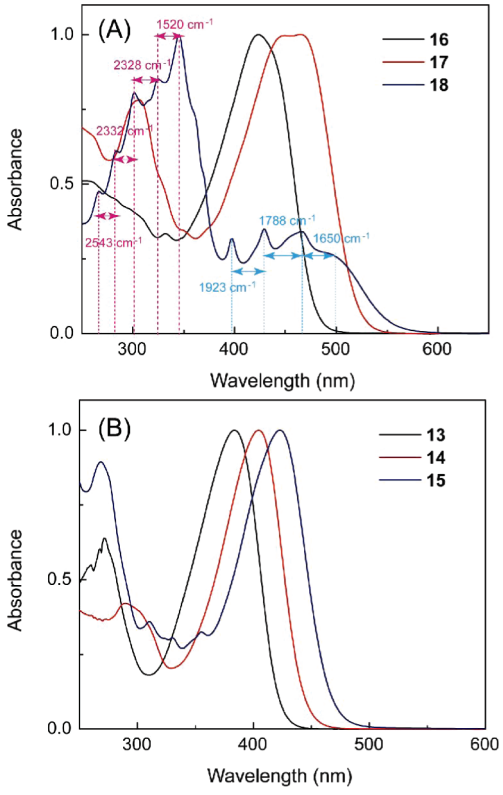

Figure 8. Normalized UV−vis spectra of (A) oligyne-exTTFs **16**−**18** and (B) acetylenic DTFs **13**−**15** measured in $CHCl_3$ at room temperature.

From Figure 8A, the low-energy cutoff absorption wavelengths of oligoyne-exTTFs **16**−**18** are clearly seen to redshift with increasing length of the oligoyne unit. A similar trend of redshift can be observed in the spectra of acetylenic DTF precursors. As shown in Figure 8B, the lowest energy absorption bands are steadily red-shifted from alkynyl-DTF **13** (λ_{max} = 383 nm) to diyne-DTF **14** (λ_{max} = 404 nm) and triyne-DTF **15** (λ_{max} = 423 nm) as a function of the number of acetylenic units attached to the phenyl-DTF group. The UV−vis data indicate that the optical bandgaps (E_g) of oligoyne-exTTFs are dependent on the chain length of the central oligoyne moiety. DFT calculations have provided rationalization for the observed electronic absorption properties. Figure 9 shows the frontier molecular orbital (FMOs) contour surfaces and energies for oligoyne-exTTFs **16**−**18** calculated at the B3LYP/6-31G* level. It can be seen that the highest occupied molecular orbitals (HOMOs) are evenly distributed across the entire molecular π-frameworks for **16**−**18**, whereas their lowest unoccupied molecular orbitals (LUMOs) appear to be more and more localized at the central oligoyne segment as the oligoyne chain length increases. Empirically, the longer the oligoyne is, the stronger its electron accepting ability. In this sense, the increasing chain length would enhance the electron "push−pull" effect between DTF (donor) and oligoyne (acceptor), which in principle should result in red-shifted electronic absorption. Quantitatively, the LUMO energy is seen to decrease more significantly than the HOMO energy, rendering a declining trend for the energy gap between HOMO and LUMO as a function of oligoyne chain length. The calculated HOMO−LUMO gaps for the oligoyne-exTTFs are in good agreement with the optical gaps obtained from their UV−vis spectra (see Table 1).

Table 1. Summary of Electronic Properties of Oligoyne-exTTFs 16−18

entry	λ_{abs}, nm (ε, 10^4 M^{-1} cm^{-1})	E_{HOMO} (eV)	E_{LUMO} (eV)	ΔE_{H-L}[a] (eV)	E_g[b] (eV)
16	423 (6.69), 332 (2.23)	−5.08	−2.04	3.04	2.61
17	467 (8.39), 307 (6.58)	−5.08	−2.33	2.75	2.39
18	506, 467, 458, 431, 346, 326, 303, 283(sh), 264(sh)	−5.21	−2.71	2.50	2.25

[a] Energy gap between HOMO and LUMO. [b] Optical energy gap obtained from the intersection between the tangential line and the baseline of the lowest energy absorption profile.

dx.doi.org/10.1021/jo2000447 |J. Org. Chem. 2011, 76, 2701–2715

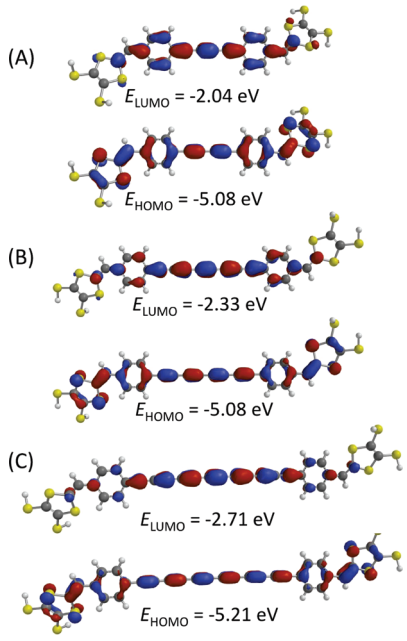

Figure 9. Plots and energies of frontier molecular orbitals (FMOs) for (A) diyne-exTTF **16**, (B) tetrayne-exTTF **17**, and (C) hexayne-exTTF **18**. Geometry optimization and single-point energy calculations were both undertaken at the B3LYP/6-31G* level, and the SMe groups were replaced by SH groups to reduce computational expenses.

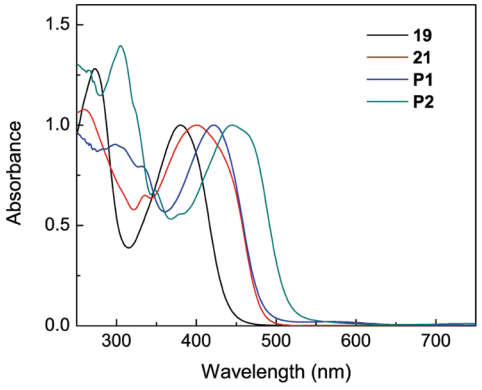

Figure 10. Normalized UV−vis spectra of compounds **19**, **21**, and polymers **P1** and **P2** measured in $CHCl_3$ at room temperature.

The UV−vis absorption properties of TTFV-based macrocycle **21**, polymers **P1** and **P1**, and their TTFV precursor **19** are compared in Figure 10. The absorption spectrum of macrocycle **21** shows three $\pi\rightarrow\pi^*$ bands at 400, 335, and 260 nm. The lowest energy band is red-shifted by ca. 20 nm relative to that of TTFV precursor **19** (λ_{max} = 380 nm) as a result of extended π-conjugation. The spectrum of polymers **P1**, which is structurally the acyclic analogue of macrocycle **21**, shows three absorption bands at 422, 331, and 298 nm, and the lowest energy absorption peak of **P1** is red-shifted by 22 nm in comparison with **21**. It is interesting to note that the low-energy cutoff edges of **21** and **P1** are nearly superimposable, which is indicative of the same optical band gap energy for the two species and suggests an insignificant degree of electronic delocalization across the acyclic π-framework of **P1**. It is therefore reasonable to assume that the TTFV units of **P1** predominately take *cis* conformation in the neutral state to form foldamers as depicted in Figure 3, since such a helical orientation would attenuate the electronic communication between each conjugated repeat segments in the polymer backbone to an extent similar to macrocycle **21**. The UV−vis spectrum of **P2** shows three absorption bands at 444, 348, and 304 nm. Compared with **P1**, the λ_{max} value of **P2** is red-shifted by 22 nm as a result of further elongated oligyne chain length. In addition to the significant $\pi\rightarrow\pi^*$ features, the spectra of **P1** and **P2** both show a weak long-wavelength hump in the vis−NIR region, peaking at 566 nm for **P1** and 738 nm for **P2**. The origins of these peaks can be attributed to trace amounts of cationic TTFV moieties due to incomplete reduction during the polymer preparation process. This assignment is corroborated by the results of spectroelectrochemical analysis (vide infra).

Electrochemical and Electrochromic Properties. The electrochemical redox properties of oligoyne-exTTFs and related compounds were investigated by cyclic voltammetric (CV) analysis, and the detailed voltammograms are given in Figure 11.

The CV profile of diyne-exTTF **16** (Figure 11A) shows an anodic peak at E_{pa} = +0.75 V and a cathodic peak at E_{pc} = +0.55 V on the first scan cycle. The anodic wave originates from the oxidation of the DTF moieties in **16** to $[DTF]^{\bullet+}$. The cathodic peak, however, is not due to a correlated reversible reduction process of $[DTF]^{\bullet+}$. Instead, it corresponds to the simultaneous bielectronic reduction on $[TTFV]^{2+}$ that results from a rapid dimerization reaction of $[DTF]^{\bullet+}$ on the electrode surface. The assignment is evidenced by the dramatically changed voltammogram patterns observed on the second CV scan cycle, in which a new anodic peak emerges at +0.62 V, preceding the anodic peak at +0.75 V. Compared with the cyclic voltammogram of TTFV precursor **19** (Figure 11C), the reversible couple at E_{pa} = +0.62 V and E_{pc} = +0.55 V can be reasonably assigned to the redox processes taking place at TTFV units. In the succeeding scan cycles, the cathodic peak due to $[DTF]^{\bullet+}$ formation (at ca. +0.75 V) shows a gradual decrease in intensity, whereas the redox wave pairs related to the TTFV groups are seen to steadily increase in intensity. This observation is indicative of electropolymerization of **16** on the surface of the working electrode to form multiple layers of conductive polymers. Indeed, after a number of CV scans, a smooth and uniform thin film was observed to be deposited on the surface of the working electrode. In Figure 11A, it is also notable that the redox wave pairs associated with the TTFV moiety show gradually increased quasi-reversible behavior with increasing number of CV scans. Tetrayne-exTTF **17** gives CV patterns (see Figure 11B) very similar to those of diyne-exTTF **16** and affords a high-quality conductive polymer thin film on the working electrode surface after successive CV scans. The voltammogram of macrocycle **21** shows a pair of quasi-reversible redox waves at E_{pa} = +0.82 V and E_{pc} = +0.56 V (Figure 11D). Compared with the voltammogram of TTFV **19**, the redox potentials of **21** are shifted anodically by ca. 0.1 V. The shift is due to the conformational constraint in macrocycle **21** that prohibits the TTFV moiety from stretching into a *trans* TTFV dication upon oxidation. Similar effects have been observed in a series of poly(ethylene glycol)-tethered TTFV macrocycles reported by Lorcy and co-workers.[89]

Clearly, the CV results show that both diyne-exTTF **16** and tetrayne-exTTF **17** are excellent precursors for preparation of conductive polymer thin film devices by electrodeposition methods.[85] To further explore this potential, we then performed electropolymerization of **16** and **17** on indium tin oxide (ITO)-coated glass substrates by means of multicycle CV scans (100

dx.doi.org/10.1021/jo2000447 |*J. Org. Chem.* 2011, 76, 2701–2715

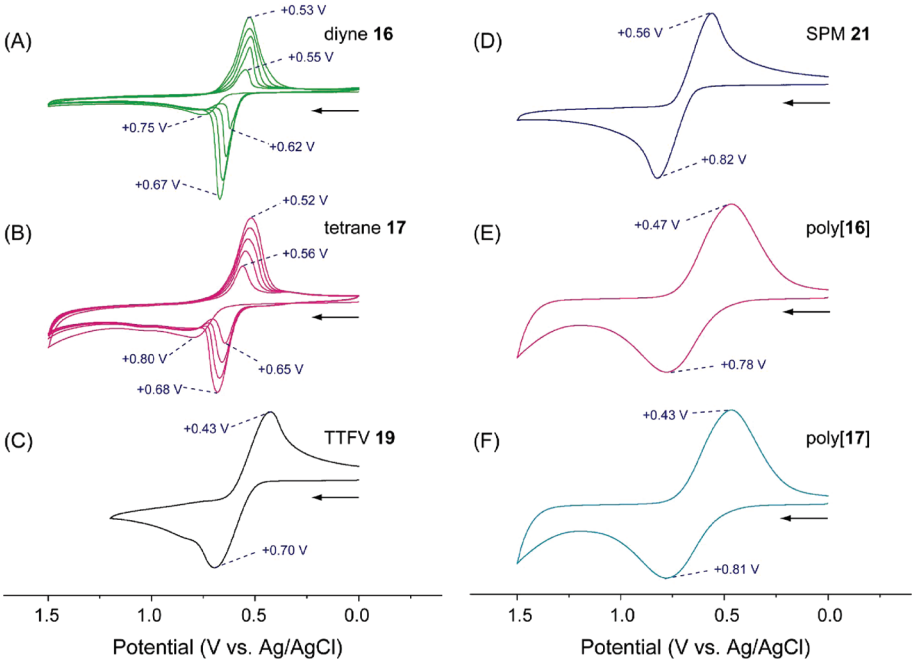

Figure 11. Cyclic voltammograms of (A) diyne-exTTF **16** (10^{-3} M), scan rate: 200 mV s^{-1}, working electrode: glassy carbon; (B) tetrayne-exTTF **17** (10^{-3} M), scan rate: 200 mV s^{-1}, working electrode: glassy carbon; (C) TTFV **19** (10^{-3} M), scan rate: 50 mV s^{-1}, working electrode: glassy carbon; (D) macrocycle **21** (10^{-3} M), scan rate: 50 mV s^{-1}, working electrode: glassy carbon; (E) poly[**16**] thin film, scan rate: 50 mV s^{-1}, working electrode: ITO glass; (F) poly[**17**] thin film, scan rate: 50 mV s^{-1}, working electrode: ITO glass. Experimental conditions: supporting electrolyte: Bu_4NBF_4 (0.1 M); solvent: CH_2Cl_2; counter electrode: Pt; reference electrode: Ag/AgCl. The arrows indicate the initial potential scan direction.

cycles at a scan rate of 50 mV s^{-1} in the presence of ca. 10^{-3} M precursor in Bu_4NBF_4 solution). Polymer thin films of good quality were obtained, and they exhibited good electrical conductivities and TTFV-related electroactivities as manifested in their cyclic voltammetric measurements (see Figure 11E, F). The cyclic voltammograms of both poly[**16**] and poly[**17**] include a pair of quasi-reversible redox waves resembling the CV profile of TTFV precursor **19**, indicating that TTFV moieties are the key components contributing to the redox activity of the polymers. It is also worth noting that the electrochemically prepared thin films of poly[**16**] and poly[**17**] were found to completely lose electrical conductivity and electroactivity after being stored in the neutral state for more than two weeks. Nevertheless, the conductivity and electroactivity could be readily reactivated by subjecting the thin films to a positive potential at +0.9 V for a few seconds. This behavior suggests that the doping effect plays a key role in dictating the conducting and redox active properties of the polymer thin films.

In addition to voltammetric properties, UV−vis spectroelectrochemical analysis on the exTTFs and related TTFV macromolecules was also conducted in order to probe their optical responses to electrochemical redox processes. In our experiments, each UV−vis spectral scan was performed after the electrolysis of an analyte at a controlled voltage for at least 90 s to ensure the electric current attained a constant value. As such, the systems examined by UV−vis spectroscopy can be deemed as having arrived at equilibrium.

Upon increasing oxidation, the lowest energy absorption band of diyne-exTTF **16** at 423 nm decreases steadily and a new broad band appears at 660 nm with relatively weak intensity (see Figure 12A). The new long-wavelength band is assigned to the characteristic absorption of $[TTFV]^{2+}$.[89,116] The trend of UV−vis spectral changes in the spectroelectrochemical analysis of **16** is similar to that of TTFV precursor **19** (Figure 12C), hence corroborating the formation of TTFV species in the process of electrochemical oxidation of diyne-exTTF **16**. For tetrayne-exTTF **17**, a substantial decrease of the absorption peak at 647 nm along with an increasing broad band at 668 nm can be observed from the spectroelectrochemical measurements (Figure 12B). The trend is similar to that of diyne **16**, indicating the electrochemical polymerization through the formation of TTFV units. Unlike the spectroelectrochemical data for diyne **16**, the UV−vis absorption profile of tetrayne **17** shows three sharp bands at 347, 377, and 408 nm when a high degree of oxidation is reached. The spacings between these bands are 2293 and 2015 cm^{-1}, which are consistent with a vibronic progression arising from the C≡C stretching mode. The vibrational spectral pattern is also clearly discernible in the UV−vis absorption spectrum of oxidized (cationic) poly[**17**] thin film, where three sharp bands can be seen at 353, 383, and 415 nm, respectively. The fine vibrational spectral features imply that oxidized (cationic) poly[**17**] possess more rigid polymeric backbone than its neutral form.

The spectroelectrochemical data for macrocycle **21** is shown in Figure 12D. As oxidation progresses, the lowest energy band at ca. 422 nm drops in intensity along with a moderate degree of redshift, while the absorption in the high-energy region (ca. 322 nm) is increased slightly. The most notable spectral variation, however, is the substantial rise of a broad absorption tail from ca. 500 to 750 nm with a barely distinguishable peak at 600 nm. This pattern is markedly different from those of acyclic TTFV species **16**, **17**, and **19**. The pronounced low-energy tail in the spectrum of oxidized macrocycle **21** is correlated to the electronic absorptions of $[TTFV]^{2+}$. Given the unique conformational constraint in macrocycle **21**, the TTFV moieties must retain *cis*-conformation even after being oxidized into $[TTFV]^{2+}$ dications. In this sense, macrocycle **21** offers a convenient model

dx.doi.org/10.1021/jo2000447 |*J. Org. Chem.* 2011, 76, 2701–2715

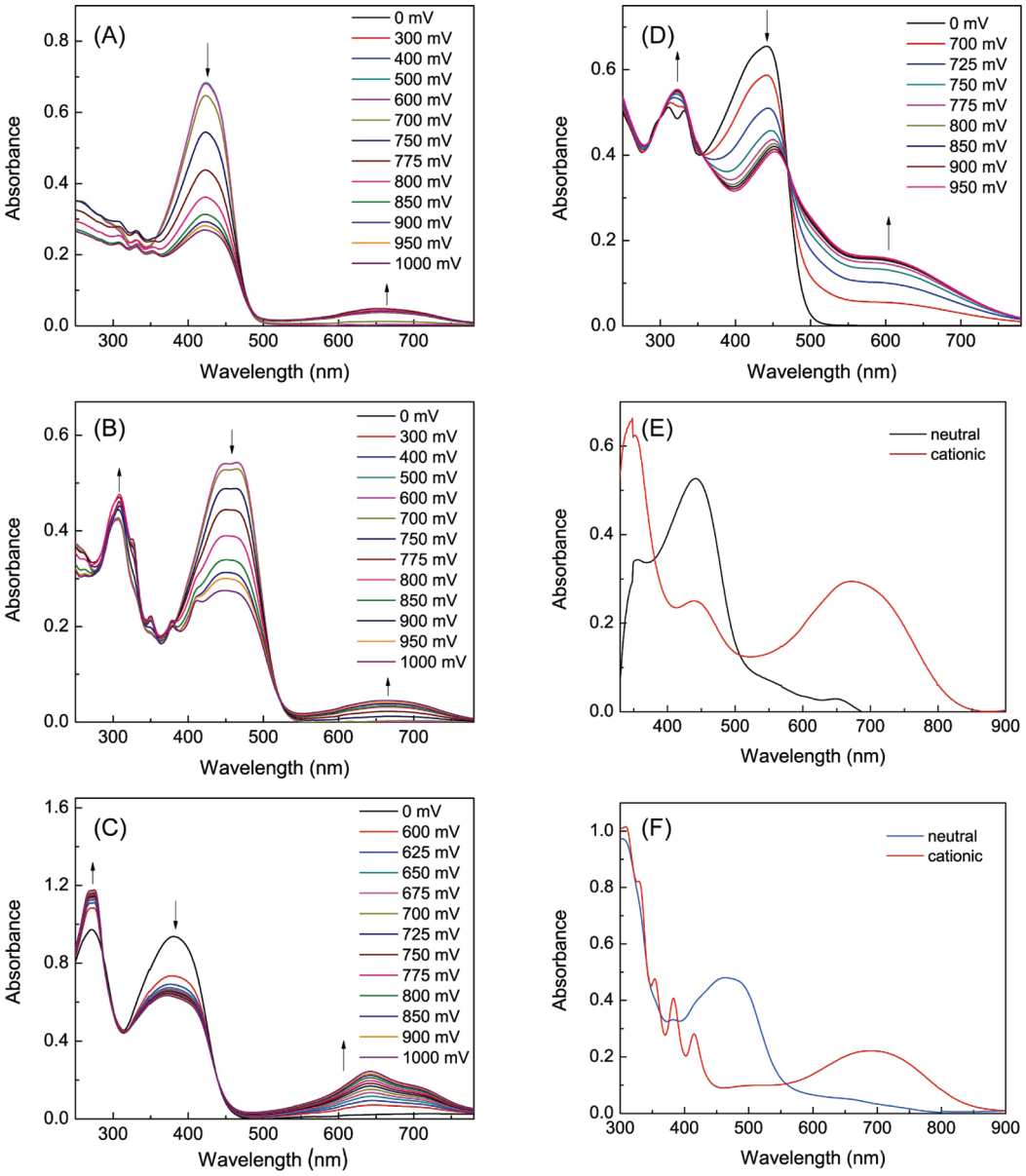

Figure 12. UV−vis spectroelectrochemistry of (A) diyne-exTTF **16** (10^{-4} M), (B) tetrayne-exTTF **17** (10^{-4} M), (C) TTFV **19** (10^{-4} M), and (D) macrocycle **21** (10^{-4} M). Experimental conditions: supporting electrolyte: Bu_4NBF_4 (0.1 M); solvent: CH_2Cl_2; working electrode: Pt mesh; counter electrode: Pt; reference electrode: Ag/AgCl. (E) UV−vis absorption spectra of poly[**16**] on ITO glass in the neutral (blue trace) and cationic (red trace) states. (F) UV−vis absorption spectra of poly[**17**] on ITO glass in the neutral (blue trace) and cationic (red trace) states.

to unravel the unique electronic absorption properties of *cis*-$[TTFV]^{2+}$.[89]

The solution-phase UV−vis spectroscopic studies have revealed that in the neutral state the synthesized TTFV-containing compounds are electronic transparent in the vis−NIR region of the spectrum (500−800 nm), whereas they become quite absorbing in this spectral range after being oxidized. In addition, the oxidation and reduction processes on the TTFV moieties are chemically reversible. Collectively, these spectral and electrochemical properties point to potential applications in electrochromism and electrochromic devices.[117−121] To further investigate the electrochromic properties in the solid state, the UV−vis absorption spectra of polymer films prepared by electrodeposition of diyne-exTTF **16** and tetrayne-exTTF **17** on ITO glass were characterized in both neutral and oxidized states. As shown in Figure 12E, the thin film of poly[**16**] shows a strongly absorbing $\pi \rightarrow \pi^*$ transition band at 441 nm. In addition, a weak absorption tail is observed in the range of ca. 500−700 nm, which likely arises from trace amounts of unreduced $[TTFV]^{2+}$ moieties (doping) in the polymer film. After being subjected to electrolysis at +0.9 V for 1 min, the thin film of poly[**16**] was observed to gradually change color from pale yellow to dark green. The UV−vis spectrum of oxidized poly[**16**] shows a strong broad low-energy band covering the spectral range of 500 to 850 nm and peaking at 670 nm (Figure 12E). Meanwhile the absorption peak at 441 nm is greatly attenuated. In the UV−vis spectrum of neutral poly[**17**] thin film (Figure 12F), a strong absorption band at 464 nm and a long absorption tail extending from ca. 550 to 800 nm are observed. Upon oxidation, the peak at 464 nm disappears, while a broad

dx.doi.org/10.1021/jo2000447 |*J. Org. Chem.* 2011, 76, 2701–2715

band appears in the vis−NIR region (ranging from 550 to 900 nm and peaking at 691 nm) together with three distinctive vibronic bands at 415, 383, and 353 nm are observed. The fine vibrational structures observed in the high-energy region are consistent with the signature vibrational mode of tetrayne and indicate that the tetrayne moieties in poly[**17**] remain intact in the solid state during redox cycles.

CONCLUSIONS

The redox-controlled conformational switching behavior of phenyl-substituted TTFV is the key to the versatile synthesis of extended π-conjugated molecular/macromolecular structures with different topologies and structural dimensions, ranging from "rod-like" oligoyne-exTTFs to TTFV-containing shape-persistent macrocycles and conducting polymer wires. The optical gaps of oligoyne-exTTFs show a reducing trend and do not converge as the oligoyne chain length increases from diyne to hexayne. X-ray structural analysis shows that the terminal DTF groups in oligoyne-exTTFs facilitate tight parallel packing of the oligoyne chains through S−S contacts, exacting a toll on the kinetic stability of higher oligoyne species. The oligoyne-exTTFs can be efficiently polymerized through DTF oxidative coupling reactions and the polymer thin films resulting from electropolymerization show intriguing conductivity and redox activities. Furthermore, the polymer films exhibit redox-switchable coloration in the Vis-NIR region of the spectrum, suggesting potential applications in electrochromic devices. The synthetic access to TTFV-oligoyne shape-persistent macrocycles **21** and **22** has not only added new members to the family of phenylacetylene-based cyclophanes but also provided useful models for better understanding the effect of conformational constraint on the electronic properties of TTFV-embedded macromolecular systems. It is also envisaged that the nearly flat arrangement of the acetylene-rich ring framework of **21** could render it a unique supramolecular host for certain metal ions and aromatic molecular guests. Investigations toward this direction are currently underway. Finally, solid-state structural and thermal analyses have shown that tetrayne-exTTF **17** can undergo topochemical polymerization more readily than diyne-exTTF **16**. This finding hints that macrocycle **22** and electrochemically induced poly[**17**], if taking the folding conformation as proposed in Figure 3, may be further cross-linked through solid-state polymerization reactions of tetraynes to form well-defined and organized 3-dimensional polymer networks such as "nanotubes". This appealing aspect awaits further studies in our future work.

EXPERIMENTAL SECTION

General Methods. Chemicals and reagents were purchased from commercial suppliers and used directly without purification. All reactions were conducted in standard and dry glassware unless otherwise noted. Evaporation and concentration were carried out with a water-aspirator. Flash column chromatography was performed using 240−400 mesh silica gel. Thin-layer chromatography (TLC) was carried out with silica gel 60 F254 covered on plastic sheets and visualized by UV light. ^{1}H and ^{13}C NMR spectra were measured on a 500 MHz spectrometer and chemical shifts are reported in ppm downfield from the signal of the internal reference $SiMe_4$. Coupling constants (J) are given in Hz. Positive-mode high-resolution mass spectra (HRMS) were measured on a mass spectrometer equipped with an electron-impact ionization (EI) ion source or a hybrid quadrupole/TOF mass spectrometer equipped with an o-MALDI ion source. All samples for thermal analyses (DSC and TGA) were measured under a nitrogen atmosphere. Cyclic voltammetric (CV) analyses were carried out in a standard three-electrode setup. Spectroelectrochemistry was investigated through the following protocol: In a 1 mm quartz cuvette were placed a Pt mesh as working electrode, a Ag/AgCl reference electrode, and a Pt wire as counter electrode. The applied potential (V) was increased in steps through controlled potential electrolysis. In each potential step, the electrolysis was first performed for ca. 1.5 min until the electrical current remained constant, then a UV−vis spectrum was determined. Quantum chemical calculations were performed using the density functional theory (DFT) and semiempirical (RM1) methods implemented in the Spartan'06 software package (Wavefunction, Inc.).

Synthesis of DTF 13. To a solution of phosphonate **11** (900 mg, 2.96 mmol) in THF (60 mL) cooled by a dry ice bath was added *n*-BuLi (1.50 mL, 2.5 M in THF, 3.75 mmol). The mixture was stirred for 20 min and then 4-(trimethylsilylethynyl)benzaldehyde (**12**) (530 mg, 2.62 mmol) in THF (20 mL) was added. The mixture was allowed to be slowly warmed up to rt and stirred overnight. The resulting dark brown yellow solution was diluted with Et_2O, washed with H_2O, and dried over $MgSO_4$. After concentration under vacuum, the residue was subjected to column chromatography (10% CH_2Cl_2 in hexanes) affording compound **13** (800 mg, 2.12 mmol, 80%) as a light yellow liquid, which slowly solidified into a yellow solid in a refrigerator: mp 90−91 °C; IR (KBr) 2954, 2920, 2149, 1563, 1540, 1499, 1247 cm^{-1}; ^{1}H NMR (500 MHz, $CDCl_3$) δ 7.45 (d, J = 8.3 Hz, 2H), 7.13 (d, J = 8.4 Hz, 2H), 6.43 (s, 1H), 2.44 (s, 3H), 2.43 (s, 3H), 0.29(s, 9H); ^{13}C NMR (125 MHz, $CDCl_3$) δ 136.7, 134.2, 132.5, 128.1, 126.9, 124.7, 120.5, 114.3, 105.8, 95.1, 19.5, 19.3, 0.5; HRMS (MALDI-TOF, +eV) m/z calcd for $C_{17}H_{21}S_4Si$ 381.0295, found 381.0306 $[M]^+$.

Synthesis of Diyne-DTF 14. To a solution of DTF **13** (95 mg, 0.25 mmol) in 20 mL of THF/MeOH (1:1) was added K_2CO_3 (200 mg, 1.45 mmol). The mixture was stirred at rt for 30 min. The mixture was diluted with CH_2Cl_2, washed with H_2O, dried over $MgSO_4$, and concentrated to 1 mL in vacuo. The residue was diluted with CH_2Cl_2 (20 mL), and to this solution were then added TMSA (0.50 mL, 3.4 × mmol) and a solution of CuI (90 mg, 0.47 mmol) and TMEDA (0.10 mL) in CH_2Cl_2 (3 mL). The mixture was stirred at rt under air for 3 h, and then it was washed with H_2O, dried over $MgSO_4$, and column chromatographed to give DTF **14** (0.83 mg, 0.21 mmol, 82%) as a yellow solid: mp 85−86 °C; IR (KBr) 2923, 2854, 2199, 2102, 1564, 1385 cm^{-1}; ^{1}H NMR ($CDCl_3$, 500 MHz) δ 7.44 (d, J = 8.5 Hz, 2H), 7.12 (d, J = 8.5 Hz, 2H), 6.43 (s, 1H), 2.43 (s, 3H), 2.42 (s, 3H), 0.22(s, 9H); ^{13}C NMR ($CDCl_3$, 125 MHz) δ 137.3, 135.1, 133.1, 128.0, 126.7, 124.7, 118.2, 113.8, 91.2, 88.2, 77.3, 74.9, 19.2, 19.1, −0.2; HRMS (EI, +eV) m/z calcd for $C_{19}H_{20}S_4Si$ 405.0295, found 405.0299 $[M]^+$.

Synthesis of Triyne-DFT 15. To a solution of diyne-DTF **14** (220 mg, 0.55 mmol) in THF/MeOH (1:1, 30 mL) was added K_2CO_3 (200 mg, 1.45 mmol). The mixture was stirred at rt for 20 min. The mixture was diluted with Et_2O, washed with H_2O, and dried over $MgSO_4$. After vacuum evaporation, the residue was redissolved in CH_2Cl_2 (20 mL). In the meantime, a solution of CuI (300 mg, 1.57 mmol) and TMEDA (0.30 mL) in CH_2Cl_2 (27 mL) was prepared. To this mixture was slowly added a premixed solution of desilylated DTF diyne **14** and TMSA (3.00 mL, 20.7 mmol) at rt under air over a period of 4 h, and then the reaction mixture was stirred for another 0.5 h, washed with H_2O, dried over $MgSO_4$, and column chromatographed (10% CH_2Cl_2 in hexanes) to afford triyne-DTF **15** (138 mg, 0.324 mmol, 59%) as a yellow solid: mp 117−118 °C; IR (KBr) 2957, 2916, 2163, 2072, 1595, 1566 cm^{-1}; ^{1}H NMR (500 MHz, $CDCl_3$) δ 7.51 (d, J = 8.0 Hz, 2H), 7.17 (d, J = 8.5 Hz, 2H), 6.47 (s, 1H), 2.47 (s, 3H), 2.46 (s, 3H), 0.25(s, 9H); ^{13}C NMR (125 MHz, $CDCl_3$) δ 137.9, 135.7, 133.7, 128.3, 127.0, 125.0, 117.6, 113.7, 89.6, 88.5, 75.4, 67.6, 62.2, 19.4, 19.3; HRMS (EI, +eV) m/z calcd for $C_{21}H_{20}S_4Si$ 428.0217 found 428.0215 $[M]^+$.

Synthesis of Diyne-exTTF 16. To a solution of DTF **13** (107 mg, 0.283 mmol) in THF/MeOH (1:1, 30 mL) was added K_2CO_3 (200 mg, 1.45 mmol). The mixture was stirred at rt for 30 min, diluted with

CH_2Cl_2, washed with H_2O, dried over $MgSO_4$, and concentrated in vacuo to ca. 2 mL. The residue was redissolved in CH_2Cl_2 (30 mL), and to the resulting yellow solution was added a solution of CuI (200 mg, 1.05 mmol) and TMEDA (0.20 mL) in CH_2Cl_2 (3 mL). The mixture was stirred at rt under air for 3 h, washed with H_2O, dried over $MgSO_4$, and concentrated in vacuo. The residue was subjected to silica flash column chromatography (10% CH_2Cl_2 in hexanes) to give diyne-exTTF **16** (57 mg, 0.093 mmol, 66%) as a yellow solid: mp >170 °C dec; IR (KBr) 2923, 2856, 1653, 1621, 1385 cm^{-1}; ^1H NMR (500 MHz, $CDCl_3$) δ 7.51 (d, J = 8.2 Hz, 4H), 7.18 (d, J = 8.2 Hz, 4H), 6.48 (s, 2H), 2.47 (s, 6H), 2.46 (s, 6H); ^{13}C NMR (125 MHz, $CDCl_3$) δ 137.3, 135.3, 133.1, 128.3, 127.0, 125.0, 119.0, 114.2, 83.0, 75.4, 19.5, 19.3; HRMS (MALDI-TOF, +eV) m/z calcd for $C_{28}H_{23}S_8$ 614.9565, found 614.9566 $[M + H]^+$.

Synthesis of Tetrayne-exTTF 17. To a solution of diyne-DTF **14** (71 mg, 0.18 mmol) in THF/MeOH (1:1, 20 mL) was added K_2CO_3 (200 mg, 1.45 mmol). The mixture was stirred at rt for 30 min, diluted with Et_2O, washed with H_2O, and dried over MgSO4. After vacuum evaporation, the residue was redissolved in CH_2Cl_2 (20 mL). To the solution was then added a solution of CuI (60 mg, 0.31 mmol) and TMEDA (0.10 mL) in CH_2Cl_2 (3 mL). The mixture was stirred at rt under air for 3 h. Another portion of CH_2Cl_2 (130 mL) was added to dissolve all the solids formed during the reaction. The solution was washed with H_2O, dried over $MgSO_4$, and filtered through a short silica plug to afford pure tetrayne-exTTF **17** (58 mg, 0.88 mmol, 100%) as a golden flake: mp 200 °C dec; IR (KBr) 2959, 2925, 2854, 2195, 1637, 1618, 1385 cm^{-1}; ^1H NMR (500 MHz, $CDCl_3$) δ7.50 (d, J = 8.0 Hz, 4H), 7.15 (d, J = 8.0 Hz, 4H), 6.45 (s, 2H), 2.45 (s, 6H), 2.44 (s, 6H); ^{13}C NMR (125 MHz, $CDCl_3$) δ 137.7, 136.2, 133.5, 128.2, 126.6, 125.0, 117.1, 113.6, 78.8, 76.0, 68.6, 64.9, 19.1, 19.0; HRMS (MALDI-TOF, +eV) m/z calcd for $C_{32}H_{22}S_8$ 661.9487, found 661.9519 $[M]^+$.

Synthesis of TTFV 19. To a solution of DTF **13** (107 mg, 0.283 mmol) in CH_2Cl_2 (20 mL) was added I_2 (260 mg, 1.02 mmol). The resulting black greenish mixture, after being stirred at rt overnight, was quenched with satd $Na_2S_2O_3$ aq solution (20 mL). The contents were kept under stirring for another 1 h, then the yellow organic layer was separated, washed with H_2O, dried over $MgSO_4$, and concentrated in vacuo. The residue was dissolved in CS_2 (2 mL) and then subjected to flash column chromatography (15% CH_2Cl_2 in hexanes) to give compound **19** (64 mg, 0.085 mmol, 60%) as a yellow liquid, which solidified into a yellow solid in the refrigerator: mp 180−181 °C; IR (neat) 2919, 2849, 2153, 1523, 1425, 1247, 839, 861 cm^{-1}; ^1H NMR (500 MHz, $CDCl_3$) δ 7.38 (d, J = 8.4 Hz, 4 H), 7.30 (d, J = 8.4 Hz, 4 H), 2.42 (s, 6 H), 2.37 (s, 6 H), 0.23 (s, 18H); ^{13}C NMR (125 MHz, $CDCl_3$) δ 138.0, 137.2, 132.5, 128.7, 126.7, 126.5, 123.8, 121.4, 105.3, 95.2, 19.13, 19.07, 0.2; HRMS (MALDI-TOF, +eV) m/z calcd for $C_{34}H_{38}S_8Si_2$ 758.0278, found 758.0272 $[M]^+$.

Synthesis of TTFV 20. To a solution of diyne-DTF **14** (56 mg, 0.14 mmol) in CH_2Cl_2 (30 mL) was added I_2 (137 mg, 0.54 mmol). The mixture was stirred at rt under air overnight, and then a satd $Na_2S_2O_3$ aq solution (20 mL) was added. The mixture was stirred for another 1 h. The organic layer was separated, washed with H_2O, dried over $MgSO_4$, and concentrated in vacuo. The residue was subjected to silica column chromatography (20% CH_2Cl_2 in hexanes) to afford compound **20** as a yellow solid (32 mg, 0.040 mmol, 60%): mp 125−127 °C; IR (KBr): 2959, 2921, 2200, 2101, 1596, 1520, 1503 cm^{-1}; ^1H NMR (500 MHz, $CDCl_3$) δ 7.41 (d, J = 8.0 Hz, 2H), 7.32 (d, J = 8.0 Hz, 2H), 2.43 (s, 3H), 2.37 (s, 3H), 0.23(s, 9H); ^{13}C NMR (125 MHz, $CDCl_3$) δ 139.5, 137.7, 133.3, 129.1, 126.4, 125.5, 123.2, 119.4, 91.3, 88.2, 77.1, 75.0, 19.2, 19.1,-0.2; HRMS (MALDI-TOF, +eV) m/z calcd for $C_{38}H_{38}S_8Si_2$ for 806.0278, found 806.0280 $[M]^+$.

Synthesis of Macrocycle 21. To a solution of TTFV **19** (64 mg, 0.085 mmol) in THF/MeOH (1:1, 30 mL) was added K_2CO_3 (300 mg, 2.17 mmol). The mixture was stirred at rt for 20 min, diluted with CH_2Cl_2, washed with H_2O, dried over $MgSO_4$, and concentrated in vacuo to ca. 2 mL. The residue was redissolved in CH_2Cl_2/acetone (1:1, 30 mL). To the resulting yellow solution was sequentially added a solution of CuI (60 mg, 0.31 mmol) and TMEDA (0.10 mL) followed by $PdCl_2(PPh_3)_2$ (10 mg, 0.015 mmol) in CH_2Cl_2 (2 mL). The mixture was refluxed under air for 5 days, washed with H_2O, dried over $MgSO_4$, and concentrated in vacuo. The residue was dissolved in CS_2 (2 mL) and subjected silica flash column chromatography (40% CH_2Cl_2 in hexanes) to afford compound **21** (9.0 mg, 0.0049 mmol, 18%) as a yellow solid: mp 210 °C dec; IR (neat) 2921, 2253, 1522, 1430, 905, 730 cm^{-1}; ^1H NMR (500 MHz, $CDCl_3$) δ 7.34−7.28 (m, 24 H), 2.45 (s, 18 H), 2.44 (s, 18 H); ^{13}C NMR (125 MHz, $CDCl_3$) δ 138.1, 133.0, 128.4, 126.7, 125.6, 123.8, 120.3, 82.8, 75.3, 19.1 (one alkenyl signal and one SCH_3 signal were not observed due to coincidental overlap); HRMS (MALDI-TOF, +eV) m/z calcd for $C_{84}H_{60}S_{24}$ 1835.7992, found 1835.8222 $[M]^+$.

Synthesis of Macrocycle 22. To a solution of TTFV **20** (31 mg, 0.039 mmol) in THF/MeOH (1:1, 20 mL) was added K_2CO_3 (200 mg, 1.45 mmol). The mixture was stirred at rt for 20 min, diluted with CH_2Cl_2 (20 mL), washed with H_2O, dried over $MgSO_4$, and concentrated in vacuo to ca. 3 mL. The residue was redissolved in CH_2Cl_2/acetone (1:1, 40 mL), and to the resulting solution was added a solution of CuI (60 mg, 0.31 mmol) and TMEDA (0.10 mL) in CH_2Cl_2 (3 mL). Then $PdCl_2(PPh_3)_2$ (10 mg, 0.15 mmol) was added. The mixture was refluxed under air for 5 days. The mixture was diluted with CH_2Cl_2, washed with satd NH_4Cl (aq) and H_2O sequentially, and then dried over $MgSO_4$. After vacuum evaporation, the residue was subjected to silica flash column chromatography (35% CH_2Cl_2 in hexanes) to afford crude product of **22**. The presence of some inextricable oligomer byproducts thwarted its complete purification.

Synthesis of Poly(diyne-TTFV)s P1. To a solution of diyne **16** (43 mg, 0.070 mmol) in CH_2Cl_2 (50 mL) was added I_2 (46 mg, 0.18 mmol). The mixture was stirred at rt overnight, resulting in a pale yellow solution with dark green precipitates. To this mixture was added satd $Na_2S_2O_3$ solution (aq 20 mL), and the content was kept under stirring for 1 h. The resulting yellow organic layer was separated, washed with H_2O, and dried over $MgSO_4$. Filtration followed by evaporation under vacuum afforded **P1** as a yellow solid (39 mg, crude yield 91%): HRMS (MALDI-TOF, +eV) m/z found 1225.9014 (m = 2), 1837.8391 (m = 3), 2450.7645 (m = 4), 3063.6956 (m = 5), 3681.4704 (m = 6), 4902.6271 (m = 8).

Synthesis of Poly(tetrayne-TTFV)s P2. To a solution of TTF tetrayne **17** (26 mg, 0.040 mmol) in CH_2Cl_2 (40 mL) was added I_2 (30 mg, 0.12 mmol). The mixture was stirred at rt overnight, and then satd $Na_2S_2O_3$ solution was added. The mixture was stirred for another 1.5 h, washed with H_2O, dried over $MgSO_4$, and evaporated in vacuo to afford **P2** (24 mg, crude yield 80%) as an orange solid: HRMS (MALDI-TOF, +eV) m/z found 1321.8988 (m = 2), 1983.8686 (m = 3), 2643.7519 (m = 4).

■ ASSOCIATED CONTENT

Supporting Information. ^1H and ^{13}C NMR spectroscopic characterizations for all new compounds, mass spectrometric data for **18**, **P1**, and **P2**, computational details for oligoyne-exTTFs **16**−**18** and macrocycle **21**, and X-ray crystallographic data for **16** and **17**. This material is available free of charge via the Internet at http://pubs.acs.org.

■ AUTHOR INFORMATION

Corresponding Author
*E-mail: yuming@mun.ca.

■ ACKNOWLEDGMENT

We thank the Natural Sciences and Engineering Research Council (NSERC) of Canada, Canadian Foundation for Innovation

(CFI), and Memorial University of Newfoundland for financial support.

REFERENCES

(1) *TTF Chemistry: Fundamentals and Applications of Tetrathiafulvalene*; Yamada, J.-i., Sugimoto, T., Eds.; Springer-Verlag: Berlin, 2004.
(2) Bryce, M. R. *J. Mater. Chem.* **2000**, *10*, 589.
(3) Wudl, F.; Smith, G. M.; Hufnagel, E. J. *Chem. Commun.* **1970**, 1435.
(4) Wudl, F.; Wobschall, D.; Hufnagel, E. J. *J. Am. Chem. Soc.* **1972**, *94*, 670.
(5) Yamada, J.-i.; Akutsu, H.; Nishikawa, H.; Kikuchi, K. *Chem. Rev.* **2004**, *104*, 5057.
(6) Frere, P.; Skabara, P. J. *Chem. Soc. Rev.* **2005**, *34*, 69.
(7) Talham, D. R. *Chem. Rev.* **2004**, *104*, 5479.
(8) Day, P.; Kurmoo, M. *J. Mater. Chem.* **1997**, *7*, 1291.
(9) Enoki, T.; Miyazaki, A. *Chem. Rev.* **2004**, *104*, 5449.
(10) Dichtel, W. R.; Miljanić, O. S.; Zhang, W.; Spruell, J. M.; Patel, K.; Aprahamian, I.; Heath, J. R.; Stoddart, J. F. *Acc. Chem. Res.* **2008**, *41*, 1750.
(11) Segura, J. L.; Martín, N. *Angew. Chem., Int. Ed.* **2001**, *40*, 1372.
(12) Canevet, D.; Sallé, M.; Zhang, G.; Zhang, D.; Zhu, D. *Chem. Commun.* **2009**, 2245.
(13) Balzani, V.; Gómez-López, M.; Stoddart, J. F. *Acc. Chem. Res.* **1998**, *31*, 405.
(14) Pease, A. R.; Jeppesen, J. O.; Stoddart, J. F.; Luo, Y.; Collier, C. P.; Heath, J. R. *Acc. Chem. Res.* **2001**, *34*, 433.
(15) Bendikov, M.; Wudl, F.; Perepichka, D. F. *Chem. Rev.* **2004**, *104*, 4891.
(16) Rovira, C. *Chem. Rev.* **2004**, *104*, 5289.
(17) Martín, N.; Sánchez, L.; Herranz, M. Á.; Illescas, B.; Guldi, D. M. *Acc. Chem. Res.* **2007**, *40*, 1015.
(18) Brédas, J.-L.; Norton, J. E.; Cornil, J.; Coropceanu, V. *Acc. Chem. Res.* **2009**, *42*, 1691.
(19) Gorgues, A.; Hudhomme, P.; Sallé, M. *Chem. Rev.* **2004**, *104*, 5151.
(20) Iyoda, M.; Hasegawa, M.; Miyake, Y. *Chem. Rev.* **2004**, *104*, 5085.
(21) Martín, N.; Ortí, E. In *Handbook of Advanced Electronic and Photonic Materials and Devices*; Nalwa, H. S., Ed.; Academic Press: Burlington, 2001; p 245.
(22) Martin, N.; Sanchez, L.; Seoane, C.; Orti, E.; Viruela, P. M.; Viruela, R. *J. Org. Chem.* **1998**, *63*, 1268.
(23) Díaz, M. C.; Illescas, B. M.; Martín, N.; Perepichka, I. F.; Bryce, M. R.; Levillain, E.; Viruela, R.; Ortí, E. *Chem.—Eur. J.* **2006**, *12*, 2709.
(24) Christensen, C. A.; Batsanov, A. S.; Bryce, M. R. *J. Org. Chem.* **2007**, *72*, 1301.
(25) Hansen, T. K.; Lakshmikantham, M. V.; Cava, M. P.; Metzger, R. M.; Becher, J. *J. Org. Chem.* **1991**, *56*, 2720.
(26) Sugimoto, T.; Awaji, H.; Sugimoto, I.; Misaki, Y.; Kawase, T.; Yoneda, S.; Yoshida, Z.; Kobayashi, T.; Anzai, H. *Chem. Mater.* **1989**, *1*, 535.
(27) Bryce, M. R.; Moore, A. J.; Tanner, B. K.; Whitehead, R.; Clegg, W.; Gerson, F.; Lamprecht, A.; Pfenninger, S. *Chem. Mater.* **1996**, *8*, 1182.
(28) Alévêque, O.; Frère, P.; Leriche, P.; Breton, T.; Cravino, A.; Roncali, J. *J. Mater. Chem.* **2009**, *19*, 3648.
(29) Chen, G.; Wang, L.; Thompson, D. W.; Zhao, Y. *Org. Lett.* **2008**, *10*, 657.
(30) Chen, G.; Dawe, L.; Wang, L.; Zhao, Y. *Org. Lett.* **2009**, *11*, 2736.
(31) Bunz, U. H. F. *Angew. Chem., Int. Ed. Engl.* **1994**, *33*, 1073.
(32) Cataldo, F. *Polyynes: Synthesis, Properties, and Applications*; Taylor & Francis: Boca Raton, 2006.
(33) Haley, M. M.; Tykwinski, R. R. *Carbon-Rich Compounds: From Molecules to Materials*; Wiley-VCH: Weinheim, 2006.
(34) Zanolli, Z.; Onida, G.; Charlier, J. C. *ACS Nano* **2010**, *4*, 5174.
(35) (a) Wang, C.; Batsanov, A. S.; Bryce, M. R.; Martín, S.; Nichols, R. J.; Higgins, S. J.; García-Suárez, V. M.; Lambert, C. J. *J. Am. Chem. Soc.* **2009**, *131*, 15647. (b) Pålsson, L.-O.; Wang, C.; Batsanov, A. S.; King, S. M.; Beeby, A.; Monkman, A. P.; Bryce, M. R. *Chem.—Eur. J.* **2010**, *16*, 1470.
(36) García-Suárez, V. M.; Lambert, C. J. *Nanotechnology* **2008**, *19*, 455203.
(37) Szafert, S.; Gladysz, J. A. *Chem. Rev.* **2003**, *103*, 4175.
(38) Tykwinski, R. R.; Kendall, J.; McDonald, R. *Synlett* **2009** 2068.
(39) Gleiter, R.; Werz, D. B. *Chem. Rev.* **2010**, *110*, 4447.
(40) Luu, T.; Elliott, E.; Slepkov, A. D.; Eisler, S.; McDonald, R.; Hegmann, F. A.; Tykwinski, R. R. *Org. Lett.* **2004**, *7*, 51.
(41) Eisler, S.; Slepkov, A. D.; Elliott, E.; Luu, T.; McDonald, R.; Hegmann, F. A.; Tykwinski, R. R. *J. Am. Chem. Soc.* **2005**, *127*, 2666.
(42) Sarkar, A.; Okada, S.; Komatsu, K.; Nakanishi, H.; Matsuda, H. *Macromolecules* **1998**, *31*, 5624.
(43) Kiji, J.; Kaiser, J.; Wegner, G.; Schulz, R. C. *Polymer* **1973**, *14*, 433.
(44) Szafert, S.; Gladysz, J. A. *Chem. Rev.* **2006**, *106*, PR1.
(45) Li, Z.; Fowler, F. W.; Lauher, J. W. *J. Am. Chem. Soc.* **2009**, *131*, 634.
(46) Enkelmann, V. *Chem. Mater.* **1994**, *6*, 1337.
(47) Ouyang, X.; Fowler, F. W.; Lauher, J. W. *J. Am. Chem. Soc.* **2003**, *125*, 12400.
(48) Lauher, J. W.; Fowler, F. W.; Goroff, N. S. *Acc. Chem. Res.* **2008**, *41*, 1215.
(49) Inayama, S.; Tatewaki, Y.; Okada, S. *Polym. J.* **2010**, *42*, 201.
(50) Luo, L.; Wilhelm, C.; Sun, A.; Grey, C. P.; Lauher, J. W.; Goroff, N. S. *J. Am. Chem. Soc.* **2008**, *130*, 7702.
(51) Zhou, N.; Zhao, Y. *J. Org. Chem.* **2010**, *75*, 1498.
(52) Ding, L.; Olesik, S. V. *Chem. Mater.* **2005**, *17*, 2353.
(53) Zhou, N.; Merschrod S, E. F.; Zhao, Y. *J. Am. Chem. Soc.* **2005**, *127*, 14154.
(54) Jahnke, E.; Lieberwirth, I.; Severin, N.; Rabe, J. P.; Frauenrath, H. *Angew. Chem., Int. Ed.* **2006**, *45*, 5383.
(55) Smith, P. P. K.; Buseck, P. R. *Science* **1982**, *216*, 984.
(56) Evsyukov, S. E.; Heimann, R. B.; Kavan, L. *Carbyne and Carbynoid Structures*; Kluwer Academic: Boston, Mass, 1999.
(57) Jarowski, P. D.; Wodrich, M. D.; Wannere, C. S.; Schleyer, P. v. R.; Houk, K. N. *J. Am. Chem. Soc.* **2004**, *126*, 15036.
(58) Kleinpeter, E.; Koch, A. *J. Phys. Chem. A* **2009**, *113*, 10852.
(59) Itzhaki, L.; Rozental, E.; Altus, E.; Basch, H.; Hoz, S. *J. Phys. Chem. A* **2008**, *112*, 12812.
(60) Rogers, D. W.; Matsunaga, N.; Zavitsas, A. A.; McLafferty, F. J.; Liebman, J. F. *Org. Lett.* **2003**, *5*, 2373.
(61) Mayo, M. L.; Gartstein, Y. N. *J. Phys. Chem. A* **2010**, *114*, 6444.
(62) Chalifoux, W. A.; McDonald, R.; Ferguson, M. J.; Tykwinski, R. R. *Angew. Chem., Int. Ed.* **2009**, *48*, 7915.
(63) Gibtner, T.; Hampel, F.; Gisselbrecht, J.-P.; Hirsch, A. *Chem.—Eur. J.* **2002**, *8*, 408.
(64) Morisaki, Y.; Luu, T.; Tykwinski, R. R. *Org. Lett.* **2006**, *8*, 689.
(65) Wang, C.; Batsanov, A. S.; West, K.; Bryce, M. R. *Org. Lett.* **2008**, *10*, 3069.
(66) Gauthier, S.; Weisbach, N.; Bhuvanesh, N.; Gladysz, J. A. *Organometallics* **2009**, *28*, 5597.
(67) Kendall, J.; McDonald, R.; Ferguson, M. J.; Tykwinski, R. R. *Org. Lett.* **2008**, *10*, 2163.
(68) Bichler, P.; Chalifoux, W. A.; Eisler, S.; Shi Shun, A. L. K.; Chernick, E. T.; Tykwinski, R. R. *Org. Lett.* **2009**, *11*, 519.
(69) Luu, T.; Medos, B. J.; Graham, E. R.; Vallee, D. M.; McDonald, R.; Ferguson, M. J.; Tykwinski, R. R. *J. Org. Chem.* **2010**, *75*, 8498.
(70) Chalifoux, W. A.; Tykwinski, R. R. *Nature Chem.* **2010**, *2*, 967.
(71) Qvortrup, K.; Andersson, A. S.; Mayer, J.-P.; Jepsen, A. S.; Nielsen, M. B. *Synlett* **2004**, 2818.
(72) Nielsen, M. B. *Synlett* **2003**, 1423.
(73) Nielsen, M. B.; Petersen, J. C.; Thorup, N.; Jessing, M.; Andersson, A. S.; Jepsen, A. S.; Gisselbrecht, J.-P.; Boudon, C.; Gross, M. *J. Mater. Chem.* **2005**, *15*, 2599.
(74) Sune Andersson, A.; Qvortrup, K.; Rossel Torbensen, E.; Mayer, J.-P.; Gisselbrecht, J.-P.; Boudon, C.; Gross, M.; Kadziola, A.; Kilså, K.; Brøndsted Nielsen, M. *Eur. J. Org. Chem.* **2005**, 3660.

(75) Khanous, A.; Gorgues, A.; Texier, F. *Tetrahedron Lett.* **1990**, *31*, 7307.
(76) Khanous, A.; Gorgues, A.; Jubault, M. *Tetrahedron Lett.* **1990**, *31*, 7311.
(77) Qvortrup, K.; Jakobsen, M. T.; Gisselbrecht, J.-P.; Boudon, C.; Jensen, F.; Nielsen, S. B.; Nielsen, M. B. *J. Mater. Chem.* **2004**, *14*, 1768.
(78) Nielsen, M. B.; Moonen, N. N. P.; Seiler, P.; Diederich, F.; Boudon, C.; Gisselbrecht, J.-P.; Gross, M. *Chem. Commun.* **2001**, 1848.
(79) Nielsen, M. B.; Utesch, N. F.; Moonen, N. N. P.; Boudon, C.; Gisselbrecht, J.-P.; Concilio, S.; Piotto, S. P.; Seiler, P.; Günter, P.; Gross, M.; Diederich, F. *Chem.—Eur. J.* **2002**, *8*, 3601.
(80) Frank, B. B.; Kivala, M.; Camafort Blanco, B.; Breiten, B.; Schweizer, W. B.; Laporta, P. R.; Biaggio, I.; Jahnke, E.; Tykwinski, R. R.; Boudon, C.; Gisselbrecht, J.-P.; Diederich, F. *Eur. J. Org. Chem.* **2010**, 2487.
(81) Ryhding, T.; Petersen, M. Å.; Kilså, K.; Nielsen, M. B. *Synlett* **2007**, 0913.
(82) Kim, S. *Angew. Chem., Int. Ed.* **2009**, *48*, 7740.
(83) Roncali, J. *J. Mater. Chem.* **1997**, *7*, 2307.
(84) Cocherel, N.; Leriche, P.; Ripaud, E.; Gallego-Planas, N.; Frère, P.; Roncali, J. *New J. Chem.* **2009**, *33*, 801.
(85) Massue, J.; Ghilane, J.; Bellec, N.; Lorcy, D.; Hapiot, P. *Electrochem. Commun.* **2007**, *9*, 677.
(86) Guerro, M.; Carlier, R.; Boubekeur, K.; Lorcy, D.; Hapiot, P. *J. Am. Chem. Soc.* **2003**, *125*, 3159.
(87) Bellec, N.; Boubekeur, K.; Carlier, R.; Hapiot, P.; Lorcy, D.; Tallec, A. *J. Phys. Chem. A* **2000**, *104*, 9750.
(88) Hascoat, P.; Lorcy, D.; Robert, A.; Carlier, R.; Tallec, A.; Boubekeur, K.; Batail, P. *J. Org. Chem.* **1997**, *62*, 6086.
(89) Massue, J.; Bellec, N.; Guerro, M.; Bergamini, J.-F.; Hapiot, P.; Lorcy, D. *J. Org. Chem.* **2007**, *72*, 4655.
(90) Guerro, M.; Lorcy, D. *Tetrahedron Lett.* **2005**, *46*, 5499.
(91) Inagi, S.; Naka, K.; Chujo, Y. *J. Mater. Chem.* **2007**, *17*, 4122.
(92) Hapiot, P.; Lorcy, D.; Tallec, A.; Carlier, R.; Robert, A. *J. Phys. Chem.* **1996**, *100*, 14823.
(93) Petersen, Å. M.; Zhu, L.; Jensen, S. H.; Andersson, A. S.; Kadziola, A.; Kilså, K.; Nielsen, M. B. *Adv. Funct. Mater.* **2007**, *17*, 797.
(94) Yamashita, Y.; Tomura, M.; Tanaka, S.; Imaeda, K. *Synth. Met.* **1999**, *102*, 1730.
(95) Yamashita, Y.; Tomura, M.; Zaman, M. B. *Chem. Commun.* **1998**, 1657.
(96) Tomura, M.; Yamashita, Y. *CrystEngComm* **2000**, *2*, 86.
(97) Yamashita, Y.; Tomura, M.; Imaeda, K. *Tetrahedron Lett.* **2001**, *42*, 4191.
(98) Hill, D. J.; Mio, M. J.; Prince, R. B.; Hughes, T. S.; Moore, J. S. *Chem. Rev.* **2001**, *101*, 3893.
(99) Zhang, W.; Moore, J. S. *Angew. Chem., Int. Ed.* **2006**, *45*, 4416.
(100) Moore, J. S. *Acc. Chem. Res.* **1997**, *30*, 402.
(101) Höger, S. *Chem.—Eur. J.* **2004**, *10*, 1320.
(102) Diederich, F.; Stang, P. J.; Tykwinski, R. R. *Modern Supramolecular Chemistry: Strategies for Macrocycle Synthesis*; Wiley-VCH: Weinheim, 2008.
(103) Chen, G.; Mahmud, I.; Dawe, L. N.; Zhao, Y. *Org. Lett.* **2010**, *12*, 704.
(104) Moore, A. J.; Bryce, M. R. *Synthesis* **1991**, 26.
(105) Moore, A. J.; Bryce, M. R. *Tetrahedron Lett.* **1992**, *33*, 1373.
(106) Shao, M.; Chen, G.; Zhao, Y. *Synlett* **2008**, *2008*, 371.
(107) Hay, A. S. *J. Org. Chem.* **1962**, *27*, 3320.
(108) Müller, H.; Salhi, F.; Divisia-Blohorn, B. *Tetrahedron Lett.* **1997**, *38*, 3215.
(109) Enozawa, H.; Hasegawa, M.; Takamatsu, D.; Fukui, K.-i.; Iyoda, M. *Org. Lett.* **2006**, *8*, 1917.
(110) Bruschi, M.; Limacher, P. A.; Hutter, J.; Lüthi, H. P. *J. Chem. Theory Comput.* **2009**, *5*, 506.
(111) Geskin, V. M.; Grozema, F. C.; Siebbeles, L. D. A.; Beljonne, D.; Brédas, J. L.; Cornil, J. *J. Phys. Chem. B* **2005**, *109*, 20237.
(112) Lundberg, M.; Siegbahn, P. E. M. *J. Chem. Phys.* **2005**, *122*, 224103.
(113) Rocha, G. B.; Freire, R. O.; Simas, A. M.; Stewart, J. J. P. *J. Comput. Chem.* **2006**, *27*, 1101.
(114) Cataldo, F.; Ursini, O.; Angelini, G.; Tommasini, M.; Casari, C. *J. Macromol. Sci., Part A: Pure Appl. Chem.* **2010**, *47*, 739.
(115) Schenning, A. P. H. J.; Arndt, J.-D.; Ito, M.; Stoddart, A.; Schreiber, M.; Siemsen, P.; Martin, R. E.; Boudon, C.; Gisselbrecht, J.-P.; Gross, M.; Gramlich, V.; Diederich, F. *Helv. Chim. Acta* **2001**, *84*, 296.
(116) Chen, G.; Bouzan, S.; Zhao, Y. *Tetrahedron Lett.* **2010**, *51*, 6552.
(117) Monk, P. M. S.; Mortimer, R. J.; Rosseinsky, D. R. *Electrochromism and Electrochromic Devices*; Cambridge University Press: Cambridge, 2007.
(118) Gomar-Nadal, E.; Mugica, L.; Vidal-Gancedo, J.; Casado, J.; Navarrete, J. T. L.; Veciana, J.; Rovira, C.; Amabilino, D. B. *Macromolecules* **2007**, *40*, 7521.
(119) Wang, C.; Batsanov, A. S.; Bryce, M. R. *Chem. Commun.* **2004**, 578.
(120) Perepichka, D. F.; Bryce, M. R.; Batsanov, A. S.; McInnes, E. J. L.; Zhao, J. P.; Farley, R. D. *Chem.—Eur. J.* **2002**, *8*, 4656.
(121) Kageyama, T.; Ueno, S.; Takimiya, K.; Aso, Y.; Otsubo, T. *Eur. J. Org. Chem.* **2001**, *2001*, 2983.